REPORT NO. DOT-TSC-UMTA-72-7

EFFECT OF FREQUENCY AND SPATIAL-HARMONICS ON ROTARY AND LINEAR INDUCTION MOTOR CHARACTERISTICS

J. STICKLER
TRANSPORTATION SYSTEMS CENTER
55 BROADWAY
CAMBRIDGE, MA. 02142

transpo 72
U.S. International Transportation Exposition
Dulles International Airport
Washington, D.C.
May 27-June 4, 1972

MARCH 1972
TECHNICAL REPORT

Prepared for:

DEPARTMENT OF TRANSPORTATION
URBAN MASS TRANSPORTATION ADMINISTRATION
WASHINGTON, D.C. 20590

The contents of this report reflect the views of the Transportation Systems Center which is responsible for the facts and the accuracy of the data presented herein. The contents do not necessarily reflect the official views or policy of the Department of Transportation. This report does not constitute a standard, specification or regulation.

1. Report No.	2. Government Accession No.	3. Recipient's Catalog No.
DOT/TSC-UMTA-72-7		

4. Title and Subtitle	5. Report Date
Effect of Frequency and Spatial-Harmonics on Rotary and Linear Induction Motor Characteristics	March, 1972
	6. Performing Organization Code
7. Author(s) John J. Stickler	8. Performing Organization Report No.
9. Performing Organization Name and Address DOT/Transportation Systems Center 55 Broadway Cambridge, Mass. 02142	10. Work Unit No. R-2709
	11. Contract or Grant No. U-201
12. Sponsoring Agency Name and Address Department of Transportation Urban Mass Transportation Administration Washington, D. C. 20590	13. Type of Report and Period Covered Technical Report
	14. Sponsoring Agency Code

15. Supplementary Notes

16. Abstract

A computer analysis is made of the effect of current and MMF airgap harmonics on the output characteristics of rotary and linear induction motors. The current harmonics accompanying thyristor-control operation are evaluated by Fourier analyzing the primary current waveforms. The agreement between the computed harmonic amplitudes and those measured on an equivalent Wye-connected rotary induction motor is reasonably good. The calculated torque harmonics, which are generally small compared with the fundamental torque, tend to be maximum at unity motor slip and at large thyristor hold-off angles.

The reduction in the output thrust of linear induction motors caused by end-effect waves is calculated for different values of circuit damping constant. The results indicate a considerable negative thrust contribution due to the end-effect waves in the region of small motor slip or synchronous speeds. A family of thrust-slip characteristics is presented for a typical linear induction motor illustrating the combined effect of frequency harmonics and spatial end-effect waves on the output performance of the motor.

17. Key Words	18. Distribution Statement
•Linear Induction Motor •Harmonic Effects •Rotary Induction Motors •Thyristor-Control •End-Effects	Approved for U.S. Government only. Transmittal of this document outside the U.S. Government must have prior approval of UMTA.

19. Security Classif. (of this report)	20. Security Classif. (of this page)	21. No. of Pages	22. Price
Unclassified	Unclassified	58	

TABLE OF CONTENTS

LIST OF ILLUSTRATIONS

LIST OF ILLUSTRATIONS (CONTINUED)

LIST OF TABLES

INTRODUCTION

The current and MMF airgap harmonics present in an induction motor produce detrimental effects on the motor performance. These effects include additional heating losses in the primary and secondary circuits and core losses in the magnetic circuit. The mechanical power developed by the motor is also reduced by braking torques associated with the harmonics propagating in a backward direction. These adverse effects may be minimized if they are taken into account in the design of the motor. The purpose of this report is to present the results of a study relating induction motor performance to the relative harmonic content in the current and MMF airgap waveforms.

The effects caused by time-harmonics are best treated separately from the effects of ripple due to nonsinusoidal distribution of the secondary current. The MMF airgap harmonics depend solely on the geometry of the machine and occur with purely sinusoidal terminal voltages.[1]

The first part of this report deals with time-harmonics that result when thyristors are used to control the speed of a rotary induction motor. A computer analysis is undertaken for a specific example of a rotary induction motor controlled by symmetrically triggered thyristors. The current and phase voltage waveforms are computed and resolved into Fourier components using numerical integration. Expressions for the instantaneous currents and phase voltages are derived by determining the appropriate eigenstate solutions of the characteristic matrix valid for each system state. The average torque-slip characteristics are then calculated for two examples of induction motors at different thyristor hold-off angles. This is followed by an evaluation of the torque-harmonics and their effect on the performance characteristics of the motor.

The second part of this report considers spatial-harmonics in linear induction motors. The importance of the end-effect waves on the thrust-slip characteristics of linear induction motors is discussed and calculations are presented for a particular motor showing the reduction in motor thrust caused by end-effect waves with different damping constants. The change in the effective secondary resistance produced by these waves is next reviewed and the secondary resistance components associated with motor thrust and secondary heating losses are computed as a function of motor slip. An estimate is then given of the relative efficiency of the linear induction motor being analyzed with that of an equivalent rotary induction motor when both are operating under rated-load conditions.

The third section of the report discusses the combined effect of time- and space-harmonics on the operational characteristics of the linear induction motor. Spatial-harmonics (end-effect contribution) are included in the analytical treatment by using the effective secondary resistance previously computed for the linear induction motor in place of the fixed value of secondary resistance assumed for the rotary induction motor. The final section summarizes the different conclusions reached as a result of this study on the effect of harmonics on induction motor performance.

TECHNICAL DISCUSSION

ROTARY-VERSUS-LINEAR INDUCTION MOTORS

The principle difference between the rotary induction motor and the linear induction motor is the fact that the airgap is closed in the former, while it is open in the latter.[2] The rotary induction motor can be regarded as a linear motor of infinite length with a fixed spatial periodicity; only one traveling wave is needed to describe its operation. The linear induction motor, on the other hand, because of its finite length requires additional current-flux waves to satisfy the boundary conditions at the motor ends. These extra end-effect waves produce braking thrusts and reduce the motor's efficiency.

Equivalent circuits for the rotary and linear induction motors are shown in Figures 1 and 2 respectively. Since transformer technology is used in this report, the stator and rotor elements will be referred to as the primary and secondary. The equivalent circuits differ only as regards the effective secondary impedance seen by the primary circuit. In the linear induction motor, the effective secondary impedance varies in a complicated manner[3] with motor slip due to the end-effect waves present in the airgap. Furthermore, the effective resistance associated with the output thrust, $R_2'(1-s)/s$, and the effective resistance R_2'' associated with heating losses in the secondary circuit vary differently with slip. Only in the limit of unity slip (zero speed) when R_2' equals R_2'' do the equivalent circuits become identical. The secondary reactance in the linear induction motor is found by equating the time-rate-of-change of the airgap flux to the voltage drop across the secondary impedance. The mutual reactance given by jX_m is the effective reactance transformed from a 3-phase to an equivalent 2-phase

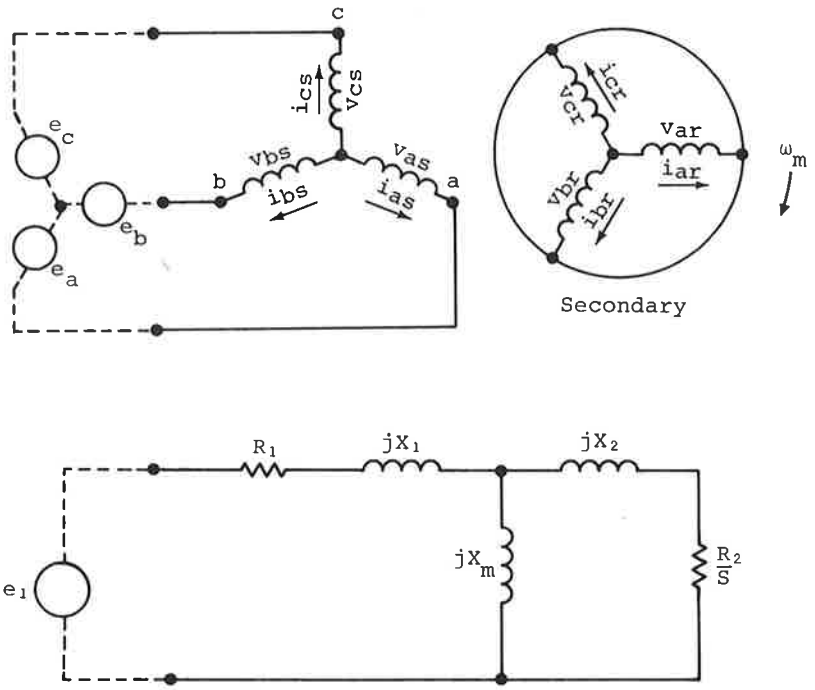

Figure 1. Schematic and Equivalent Circuit of Rotary Induction Motor

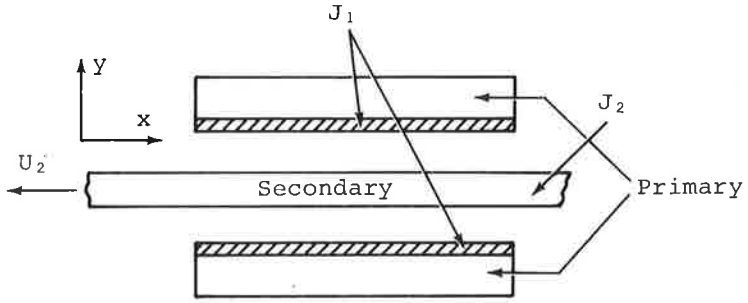

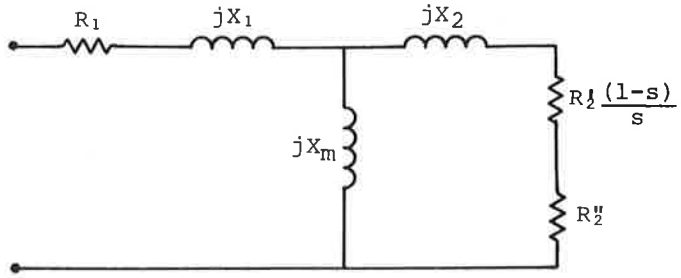

Figure 2. Schematic and Equivalent Circuit of Linear Induction Motor

system. It is equal to 3/2 times the specific mutual reactance[4] of a 3-phase winding, or the reactance measured between two inputs of the stator winding with the third open.

The equivalent circuits in Figures 1 and 2 represent one phase of the motor and the total force computed from the equivalent circuit must be multiplied by the number of phase windings in the motor. For a linear induction motor having primary windings on both sides of the reaction rail, the total thrust is twice the force computed for one side.

The secondary impedance as defined in the equivalent circuits corresponds to the transformed secondary impedance as seen by the primary circuit. For a linear induction motor having a linear reaction rail as the secondary element, the effective secondary impedance is related to the specific resistance ρ_2 and reactance ωL_{22} of the reaction rail by[3] (p. 4-12).

$$R_2 = \frac{3\ell_1 C^2 K_w^2(n)\rho_2}{P\tau_p} \qquad (1)$$

$$X_2 = \frac{P\tau_p \omega L_{22}}{3\ell_1 C^2 K_w(n)} \qquad (2)$$

where $K_w(n)$ is the winding distribution factor[5] associated with the n-th harmonic, τ_p is the pole pitch, ℓ_1 is the winding stack height, and C is the number of conductors per phase.

The equivalent circuits in Figures 1 and 2 are valid at each harmonic frequency of a repetitive input signal if the reactive impedances are multiplied by the harmonic number, n, and the slip, s, is replaced by an effective slip, s*,(see note below)

---

s* = (n-1+s)/n for slip of harmonics with positive sense of rotation
= (n+1-s)/n for slip of harmonics with negative sense of rotation

for the respective harmonic. At the higher[1] (p. 157) frequencies, it is necessary to include the increase in motor resistance caused by the skin effect. Since the latter depends upon the physical parameters characterizing the particular motor, corrections for this effect will not be attempted in the report.

In order to study in a quantitative manner the effect of harmonics on the performance of induction motors, it is helpful to examine in detail the characteristics of several specific induction machines. The induction motors chosen for this study include a Class A linear induction motor designed for use in a tracked-air-cushion-research-vehicle (Motor #1), a Class D rotary induction motor characterized by a high starting torque (Motor #2), and an additional Class D rotary induction motor which presently is being used for laboratory tests in the Power and Propulsion Branch of TSC (Motor #3). The number of poles in the above motors is equal to four. The results of the analysis on these motors are compatible and lead to conclusions which are valid for different classes of induction motors.

The impedance parameters on a per-unit-basis are given below for the three examples of induction motors.[6,7,8]

Motor #1	$R_1 = .0185$	$R_2 = .0386$	$X_1 = .144$
	$X_2 = .053$	$X_m = 1.215$	
Motor #2	$R_1 = .0566$	$R_2 = .125$	$X_1 = .063$
	$X_2 = .063$	$X_m = 1.032$	
Motor #3	$R_1 = .0088$	$R_2 = .125$	$X_1 = .09$
	$X_2 = .09$	$X_m = 2.53$	

The sections which follow are devoted to a computer study of the rotary and linear induction motors based on the equivalent circuits of Figures 1 and 2. Time-harmonics in a rotary induction motor will be considered first using the model of a 3-phase, Wye connected motor as the basis for the study analysis.

TIME-HARMONICS IN A ROTARY INDUCTION MOTOR

This treatment of time-harmonics in a 3-phase, Wye connected induction motor follows the analysis by T. A. Lipo[7] on this subject. Each phase winding of the primary motor is assumed to be connected through back-to-back pairs of thyristors to a balanced 3-phase power source. Stator (primary) voltage control is achieved by alternately open-circuiting the three stator phases at instants of zero current.

Several assumptions are made. 1) The power source is represented by a set of balanced sinusoidal 3-phase voltages having zero impedance. 2) The six thyristors have identical characteristics, with infinite impedance in the blocking mode and zero impedance in the conductive mode. 3) Balanced sets of currents flow in the motor windings and produce a single sinusoidal MMF propagating wave in space. 4) Machine parameters are assumed constant and saturation of the magnetic circuit is neglected.

The phase relationships describing the current conduction in the motor windings are shown in Figure 3. The phase current typically lags its respective line-to-neutral voltage by a phase angle ϕ (assuming an inductive load), and the delay from the point of zero phase voltage to the conduction of the succeeding thyristor in that phase is the delay angle α. The hold-off angle $\gamma=\alpha-\phi$, is the phase angle measured from the instant the phase current reaches zero to the firing of the succeeding thyristor. The decrease in thyristor angle measured with respect to the point of initial current conduction in the phase winding is β. It is related to the hold-off angle γ according to

$$\gamma + 2\beta = 120° \qquad (3)$$

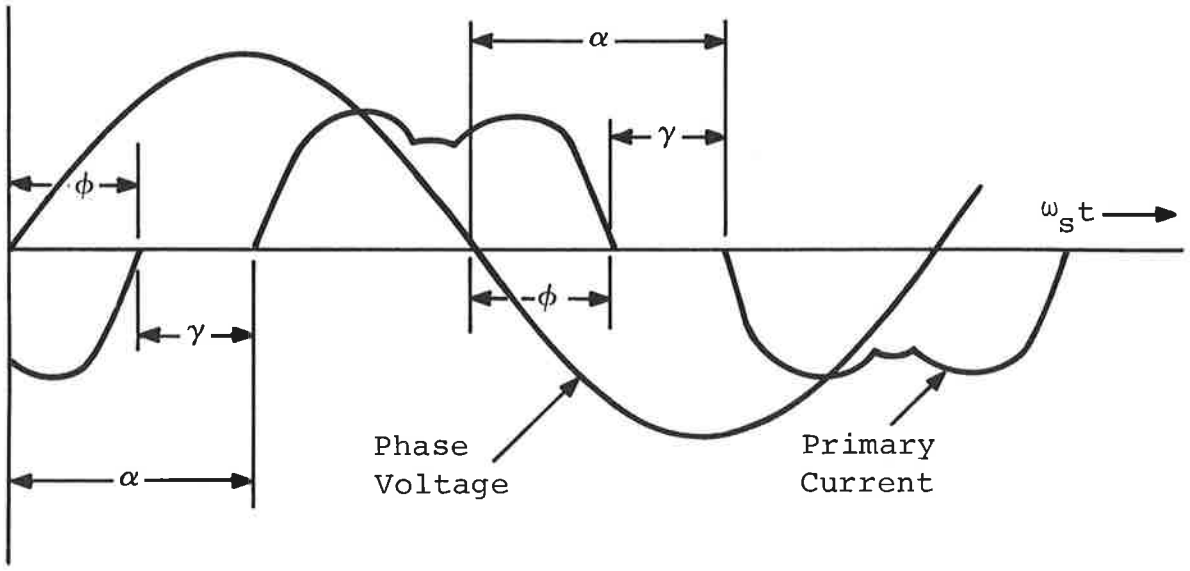

Figure 3. Current Phase Relationships in Thyristor-Controlled Induction Motor

In the discussion that follows, reference will be made to three System States: System State 1, current flows in all three windings, System State 2, current flow in one phase winding is zero, and current flow in the other two windings is nonzero, and System State 3, current flow in all three phase windings is zero.

It is useful to transform[9] the equations which describe the behavior of the machine to d-q axes fixed on the primary. This replaces time-varying coefficients in the differential equations with constant coefficients. The four simultaneous equations relating the current components along the orthoginal axes to the applied voltage V, can be written in matrix form as[7] (p. 517)

$$V = \frac{X}{\omega_s} \cdot \frac{dI}{dt} + R \cdot I \qquad (4)$$

where X and R are 4 x 4 reactance and resistance matrices, V and I are 4-dimensional voltage and current vectors, and ω_s is the angular frequency of the power supply. The solution of Equation 4 is the exponential matrix[10]

$$x(\omega t) = e^{\omega_s t \cdot A}\, x(\omega t_o) \tag{5}$$

with

$$x = \left[i_{qs}, i_{ds}, i_{qr}, i_{dr}, V_{qs}, V_{ds}\right]^T \tag{6}$$

$$A = \left[\begin{array}{c|cc} -X^{-1}\cdot R & X^{-1}\cdot C \\ \hline 0 & \begin{array}{cc} 0 & 1 \\ -1 & 0 \end{array} \end{array}\right] \tag{7}$$

The explicit forms of these matrices are given in Appendix A for the different System States. The final waveform solution given by Equation 5 must satisfy the boundary conditions for each System State as well as the rotational symmetry properties characterizing the 3-phase rotary induction motor.

A computer program was written in 7094 language to calculate the boundary state wavefunctions for each System State and compute, by an iterative process, the instantaneous phase currents and voltages within the System States. Included in the computer program is a subroutine to evaluate the first six Fourier harmonics of the primary current and phase voltage supplied to the motor.

Current-Voltage Waveforms

The instantaneous phase currents and voltages were computed at 2.5 degree phase intervals for Motor #1 for different values of thyristor hold-off angle and motor slip. Figure 4 shows the primary and secondary currents for hold-off angles of 15, 30, 45, and 60 degrees and a slip of 0.2. The waveforms computed for other values of motor slip differ only in amplitude from those presented in Figure 4. This is primarily attributable to the fact that the impedance seen by the higher current-harmonics tends to be independent of slip. The distortion in current waveform accompanying the decrease in motor current is apparent. The average phase current (as well as average torque) becomes very small for thyristor hold-off angles greater than 60 degrees.

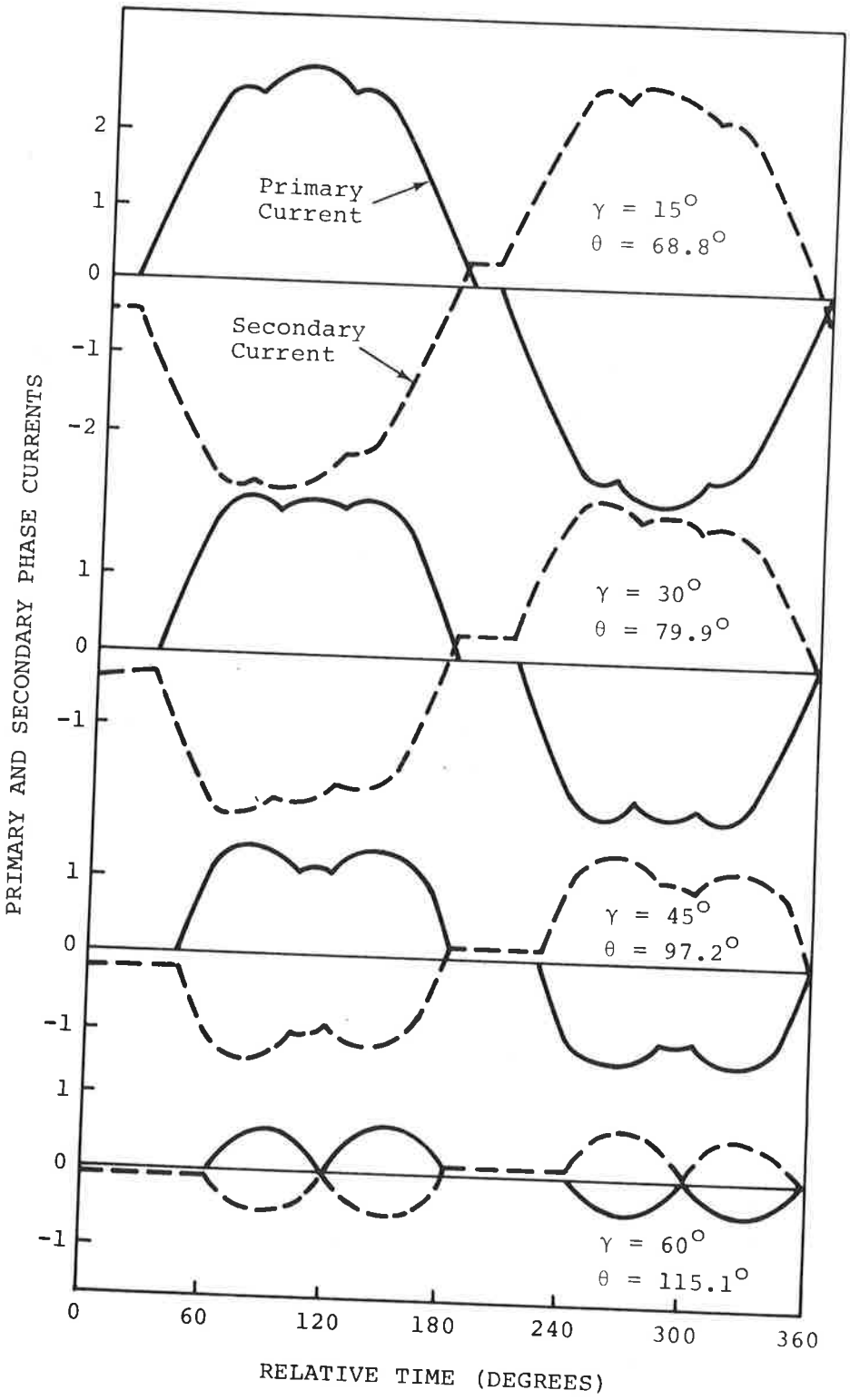

Figure 4. Current Waveforms Computed for Motor #1 at Slip of 0.2

The amplitude of the 1st harmonic (primary current) at the thyristor hold-off angle of 60 degrees is only 9 percent of its original amplitude at zero thyristor hold-off angle.

Additional waveforms were computed to illustrate the relative effect of motor slip on the shape of the voltage and current waveforms. Figure 5 shows the instantaneous phase voltage and current waveforms computed for Motor #1 for the thyristor hold-off angle of 60 degrees and motor slips of 0.03 and 0.8. The figure illustrates the pronounced effect of motor slip on the voltage waveform. Near zero slip or speeds approaching synchronous velocity, the voltage waveform approximates roughly that of the input supply voltage, shown as the dotted curve in the figure. At unity slip, the voltage waveform differs considerably from the supply voltage waveform and consists of sinusoidal segments displaced in phase with respect to each other.

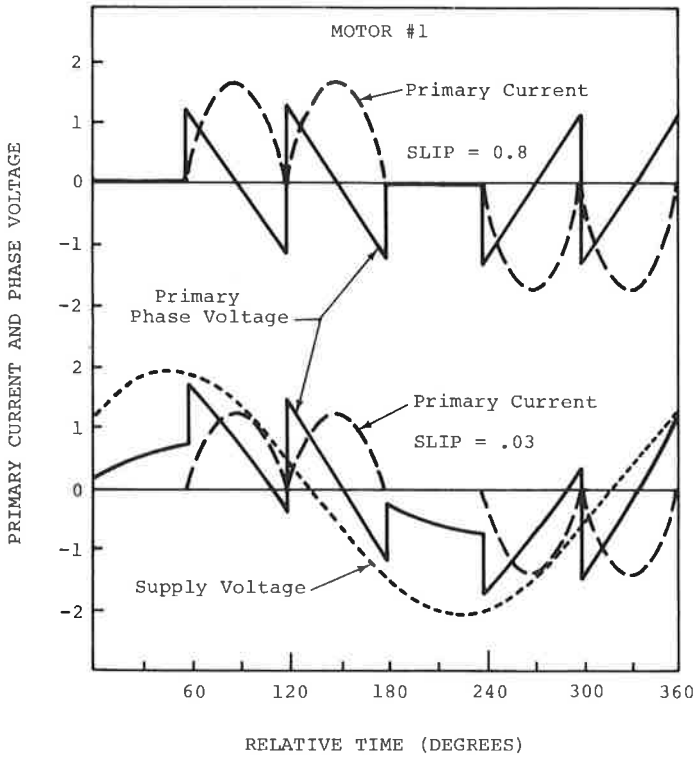

Figure 5. Phase Voltage and Current Waveforms Computed for Motor #1 at Slip of .03 and 0.8

The current waveform can be expressed in closed form as the sum of damped sinusoids representing the eigenstate solutions of the characteristic matrix A defined in Equation 7 . The complex eigenroots, $\lambda=\lambda_r \pm j\lambda_i$, specify the damping constant, λ_r, and the angular frequency, λ_i, characterizing the eigenstate solution. Figures 6 and 7 show the six eigenroots of the characteristic matrix computed for Motor #1 for System States 1 and 2 respectively. The values of slip at 0.2 intervals are indicated in the figure. The eigenroots are symmetric about the real axis and are excluded from the positive half of the real domain.

The 6 x 6 characteristic matrix describing System State #1 is reduceable to two 3 x 3 submatrices when the current-voltage vectors, defined in Equation 4 , are expressed in terms of symmetrical components[5] (p. 404). The phase currents in State #1 can then be written as the sum of the three eigenstate solutions of the reduced matrix. In System State 2, a similiar reduction of the characteristic matrix using symmetrical components is not possible. The phase currents must therefore, be expressed by a linear combination of all the eigenstate solutions of the unreduced matrix.

The expressions for the primary and secondary phase currents were determined by finding the combination of eigenstate solutions satisfying the required boundary conditions for each System State[10]. The waveforms shown in Figure 5 were chosen for representation in closed form. The equations describing the currents for Motor #1 (thyristor hold-off angle = 60 degrees; slip = 0.03, 0.8) are given in Table 1 for the phase interval $0 \leq \omega t \leq \pi/3$. The equivalent relations valid in the other phase regions are found using the transformations prescribed in the figure.

The primary and secondary current can be expressed as the sum of three terms comprising a damped and undamped sinusoid plus a damped exponential. The angular frequency of the damped

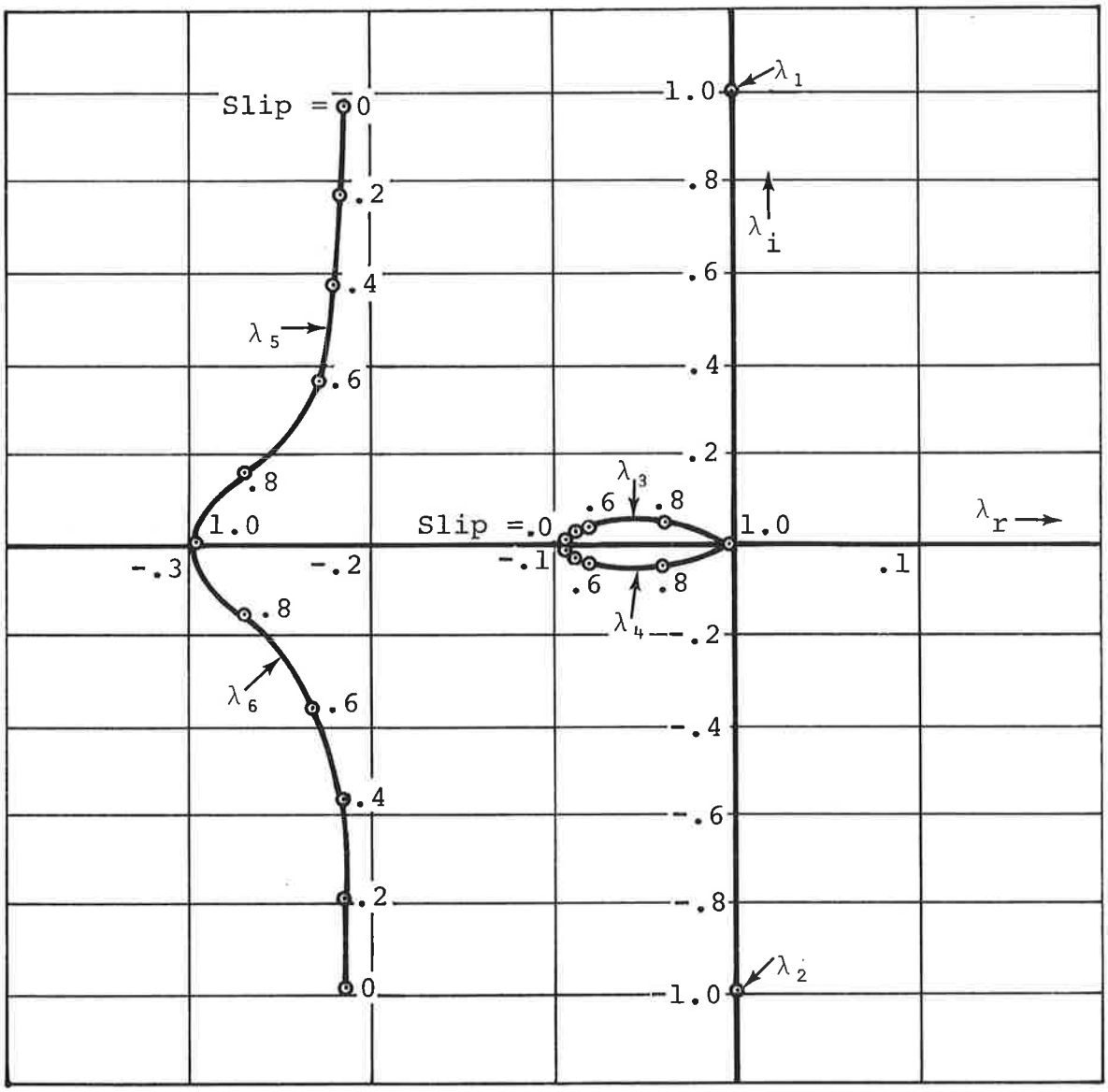

Figure 6. Complex Eigenroots of Characteristic Matrix for System State 1

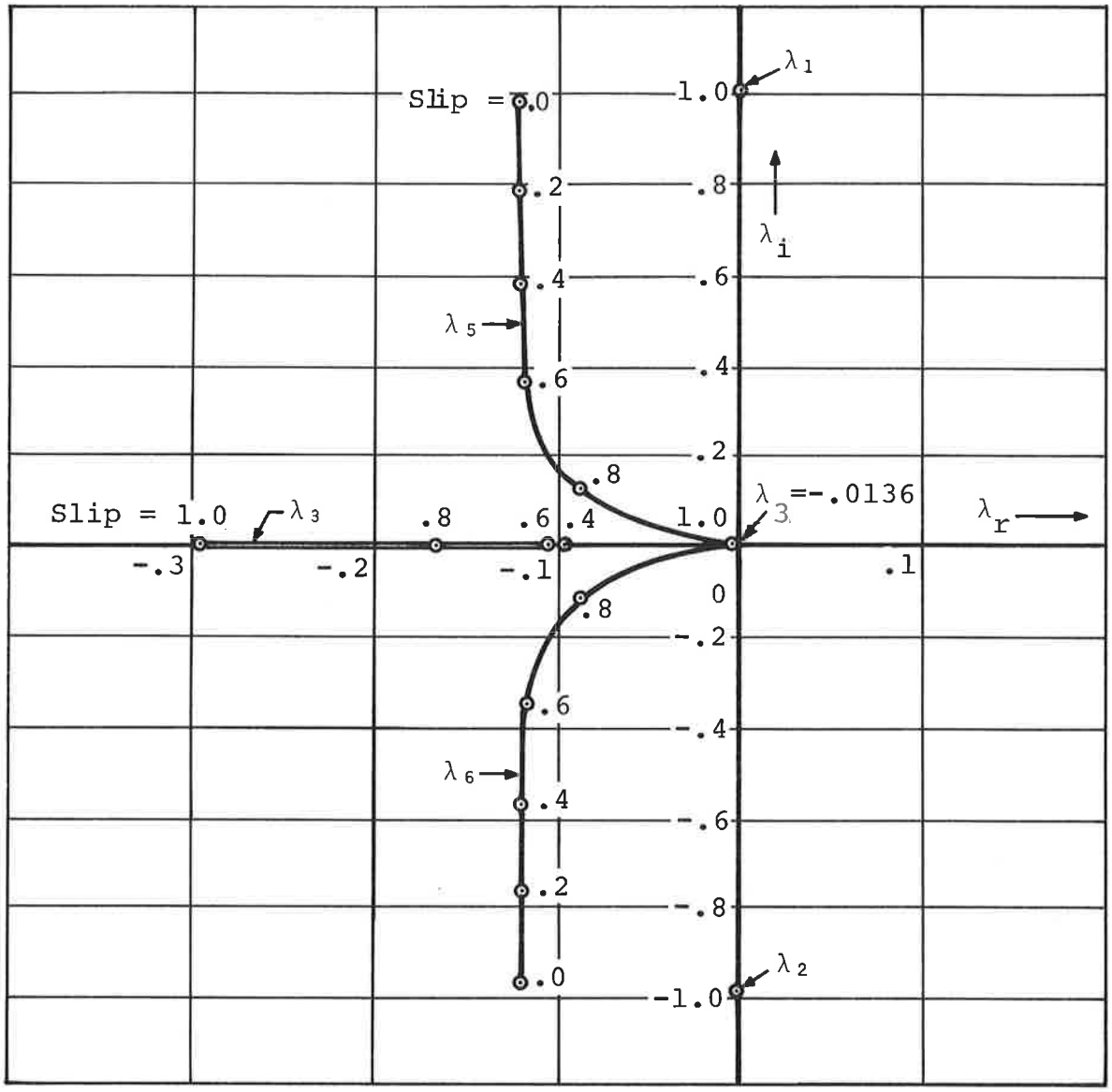

Figure 7. Complex Eigenroots of Characteristic Matrix for System State 2

TABLE 1. EQUATIONS FOR PRIMARY AND SECONDARY CURRENTS IN PHASE WINDINGS OF MOTOR #1

Hold-Off Angle (γ) = 60° Slip (s) = 0.8 $v_{supply} = \sqrt{2}\sin(\omega_s t+58.3°)$

1. $0 \leq \omega_s t \leq 60°$

$$i_{as}(\omega_s t) = 0$$

$$i_{bs}(\omega_s t) = -6.01\cos(\omega_s t-15.9°) + 9.18e^{-.087\omega_s t}\cos(.127\omega_s t+1.0°) + 15.0e^{-.164\omega_s t}$$

$$i_{cs}(\omega_s t) = -i_{bs}(\omega_s t)$$

$$i_{ar}(\omega_s t) = -.042\cos(\omega_s t-12.4°) = 2.02e^{-.087\omega_s t}\cos(.127\omega_s t+29.1°) - 1.75e^{-.164\omega_s t}$$

$$i_{br}(\omega_s t) = 5.78\cos(\omega_s t-14.1°) + 8.88e^{-.087\omega_s t}\cos(.127\omega_s t+0.6°) - 14.5e^{-.164\omega_s t}$$

$$i_{cr}(\omega_s t) = -5.78\cos(\omega_s t-14.1°) - 10.67e^{-.087\omega_s t}\cos(.127\omega_s t+5.7°) + 16.22e^{-.164\omega_s}$$

2. $60° \leq \omega_s t \leq 120°$

$$i_{as}(\omega_s t) = -i_{bs}(\omega_s t-60°);\ i_{ps}(\omega_s t) = -i_{cs}(\omega_s t-60°);\ i_{cs}(\omega_s t) = -i_{as}(\omega_s t-60°)$$
$$i_{ar}(\omega_s t) = -i_{br}(\omega_s t-60°);\ i_{br}(\omega_s t) = -i_{cr}(\omega_s t-60°);\ i_{cr}(\omega_s t) = -i_{ar}(\omega_s t-60°)$$

3. $120° \leq \omega_s t \leq 180°$

$$i_{as}(\omega_s t) = i_{cs}(\omega_s t-120°);\ i_{bs}(\omega_s t) = i_{as}(\omega_s t-120°);\ i_{cs}(\omega_s t) = i_{bs}(\omega_s t-120°)$$
$$i_{ar}(\omega_s t) = i_{cr}(\omega_s t-120°);\ i_{br}(\omega_s t) = i_{ar}(\omega_s t-120°);\ i_{cr}(\omega_s t) = i_{br}(\omega_s t-120°)$$

Hold-Off Angle (γ) = 60° Slip (s) = 0.03 $v_{supply} = \sqrt{2}\sin(\omega_s t+48.1)$

1. $0 \leq \omega_s t \leq 60°$

$$i_{as}(\omega_s t) = 0$$

$$i_{bs}(\omega_s t) = -2.10\cos(\omega_s t-8.9°) - 3.28e^{-.121\omega_s t}\cos(.957\omega_s t-41.5°) + 4.53e^{-.096\omega_s t}$$

$$i_{cs}(\omega_s t) = -i_{bs}(\omega_s t)$$

$$i_{ar}(\omega_s t) = -.812\cos(\omega_s t+37.4° + .608e^{-.121\omega_s t}\cos(.957\omega_s t+37.6°) - .157e^{-.096\omega_s t}$$

$$i_{br}(\omega_s t) = 2.34\cos(\omega_s t+19.3°) + 3.60e^{-.121\omega_s t}\cos(.957\omega_s t-51.8°) - 4.27e^{-.096\omega_s t}$$

$$i_{cr}(\omega_s t) = -1.13\cos(\omega_s t-13.3°) - 3.82e^{-.121\omega_s t}\cos(.957\omega_s t-33.3°) + 4.43e^{-.096\omega_s t}$$

2. $60° \leq \omega_s t \leq 120°$

$$i_{as}(\omega_s t) = -i_{bs}(\omega_s t-60°);\ i_{ps}(\omega_s t) = -i_{cs}(\omega_s t-60°);\ i_{cs}(\omega_s t) = -i_{as}(\omega_s t-60°)$$
$$i_{ar}(\omega_s t) = -i_{br}(\omega_s t-60°);\ i_{br}(\omega_s t) = -i_{cr}(\omega_s t-60°);\ i_{cr}(\omega_s t) = -i_{ar}(\omega_s t-60°)$$

3. $120° \leq \omega_s t \leq 180°$

$$i_{as}(\omega_s t) = i_{cs}(\omega_s t-120°);\ i_{bs}(\omega_s t) = i_{as}(\omega_s t-120°);\ i_{cs}(\omega_s t) = i_{bs}(\omega_s t-120°)$$
$$i_{ar}(\omega_s t) = i_{cr}(\omega_s t-120°);\ i_{br}(\omega_s t) = i_{ar}(\omega_s t-120°);\ i_{cr}(\omega_s t) = i_{br}(\omega_s t-120°)$$

sinusoid is roughly proportional to the angular velocity of the motor. The form of the current equations depends critically on slip, as shown by comparing the coefficients in the equations for the two values of slip. At unity slip, some simplification results in the form of the solution for System State 2 since in this case the eigenroots consist of a pure imaginary term plus two real terms. The currents are then given by two damped exponentials and one undamped sinusoid.

Next, the corresponding expressions for the primary phase voltages were derived for this example of a Wye-connected rotary induction Motor #1. The derivation makes use of the fact that the sum of the phase voltages in all three windings is zero. In System State 1 (current flows in all windings), the phase voltages are equal to the input line-to-ground supply voltages. In System State 2 (current flow in one phase winding is zero), the phase voltage across the primary winding in the blocked mode is equal to the induced voltage

$$V_a = \frac{X_m}{\omega_s} \frac{di_{qr}}{dt} \tag{8}$$

The sum of the amplitudes of the remaining two phase voltages is $\sqrt{3}$ times the d component of phase voltage. In System State 3 (current flow in all three primary windings is zero), the primary phase voltages are given by

$$V_a = \frac{X_m}{\omega_s} \frac{di_{qr}}{dt} \tag{9}$$

$$V_b = \frac{X_m}{\omega_s} \frac{d}{dt} \left(-\frac{1}{2} i_{qr} - \sqrt{\frac{3}{2}} i_{dr} \right) \tag{10}$$

$$V_c = \frac{X_m}{\omega_s} \frac{d}{dt} \left(-\frac{1}{2} i_{qr} + \sqrt{\frac{3}{2}} i_{dr} \right) \tag{11}$$

The equations for the primary voltage waveforms shown in Figure 5 are summarized in Table 2 for Motor #1 with the thyristor hold-off angle of 60 degrees and slips of .03 and .80. The phase voltages depend considerably on the voltages induced in the primary windings. When the latter are small, the voltage equations can be approximated by sinusoids having a phase displacement angle ϕ. This approximation becomes better at small slips or motor speeds approaching synchronous speed.

Torque-Slip Characteristic

The instantaneous torque with peak rated line-to-neutral voltage and peak rated line current chosen as base quantities is[7(p.517)]

$$T = X_m\left(i_{qs}\cdot i_{dr} - i_{qr}\cdot i_{ds}\right) \qquad (12)$$

where the d-q current components are found from the solution of Equation 5. The average torque is found by time-averaging the instantaneous torque over one period. Figure 8 shows the average torque-slip characteristic computed for Motor #1 for different thyristor hold-off angles. As the hold-off angle is increased, the average torque decreases and the peak average-torque shifts towards smaller motor slips. Figure 8 also compares a thyristor-control characteristic with a corresponding line-voltage characteristic. The dashed curve gives the average torque with the line-voltage reduced by 15 percent. At large motor slips, the decrease in average torque with thyristor-control is noticeably greater than with line-voltage-control.

To study the effect of thyristor-control on the output characteristics of other classes of induction motors, torque calculations were made of the Class D induction motor (Motor #2) prescribed in the second section. Figure 9 shows the torque-slip characteristics computed for this motor at different

TABLE 2. EQUATIONS FOR PRIMARY PHASE VOLTAGES IN MOTOR #1

Hold-Off Angle (γ) = 60° Slip (s) = 0.8 $v_{supply} = \sqrt{2}\sin(\omega_s t+58.3°)$

1. $0 \leq \omega_s t \leq 60°$

$$v_{as}(\omega_s t) = .051\sin(\omega_s t-12.4°) - .377e^{-.087\omega_s t}\cos(.127\omega_s t-26.5°) + .349e^{-.164\omega_s t}$$

$$v_{bs}(\omega_s t) = -1.22\cos(\omega_s t+55.8°) + .188e^{-.087\omega_s t}\cos(.127\omega_s t-26.5°) - .175e^{-.164\omega_s t}$$

$$v_{cs}(\omega_s t) = 1.22\cos(\omega_s t+61.8) + .188e^{-.087\omega_s t}\cos(.127\omega_s t-26.5°) - .175e^{-.164\omega_s t}$$

2. $60° \leq \omega_s t \leq 120°$

$$v_{as}(\omega_s t) = -v_{bs}(\omega_s t-60°)$$

$$v_{bs}(\omega_s t) = -v_{cs}(\omega_s t-60°)$$

$$v_{cs}(\omega_s t) = -v_{as}(\omega_s t-60°)$$

3. $120° \leq \omega_s t < 180°$

$$v_{as}(\omega_s t) = v_{cs}(\omega_s t-120°)$$

$$v_{bs}(\omega_s t) = v_{as}(\omega_s t-210°)$$

$$v_{cs}(\omega_s t) = v_{bs}(\omega_s t-120°)$$

Hold-Off Angle (γ) = 60° Slip (s) = 0.03 $v_{supply} = \sqrt{2}\sin(\omega_s t+48.1°)$

1. $0 \leq \omega_s t \leq 60°$

$$v_{as}(\omega_s t) = .986\sin(\omega_s t+37.4°) - .713e^{-.121\omega_s t}\cos(.957\omega_s t-45.2°) + .018e^{-.096\omega_s t}$$

$$v_{bs}(\omega_s t) = -1.40\cos(\omega_s t+68.4°) + .357e^{-.121\omega_s t}\cos(.957\omega_s t-45.2°) - .009e^{-.096\omega_s t}$$

$$v_{cs}(\omega_s t) = 1.23\cos(\omega_s t+24.8°) + .357e^{-.121\omega_s t}\cos(.957\omega_s t-45.2°) - .009e^{-.096\omega_s t}$$

2. $60 \leq \omega_s t \leq 120°$

$$v_{as}(\omega_s t) = -v_{bs}(\omega_s t-60°)$$

$$v_{bs}(\omega_s t) = -v_{cs}(\omega_s t-60°)$$

$$v_{cs}(\omega_s t) = -v_{as}(\omega_s t-60°)$$

3. $120° \leq \omega_s t \leq 180°$

$$v_{as}(\omega_s t) = v_{cs}(\omega_s t-120°)$$

$$v_{bs}(\omega_s t) = v_{as}(\omega_s t-120°)$$

$$v_{cs}(\omega_s t) = v_{bs}(\omega_s t-120°)$$

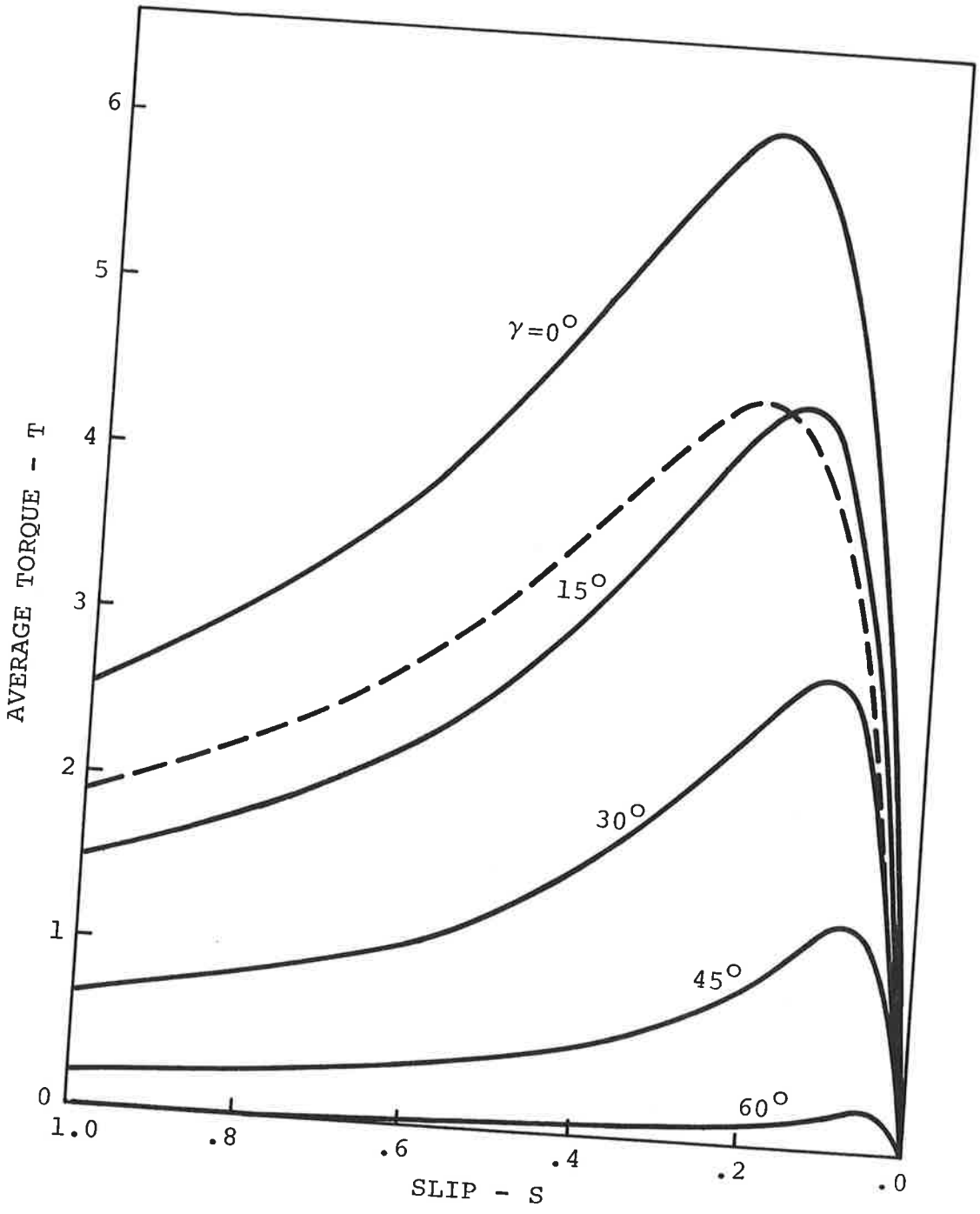

Figure 8. Torque-Slip Characteristics of Rotary Induction Motor #1 with Thyristor-Control. Dashed Curve Corresponds to Line Voltage-Control with Supply Voltage Reduced by 15 Percent

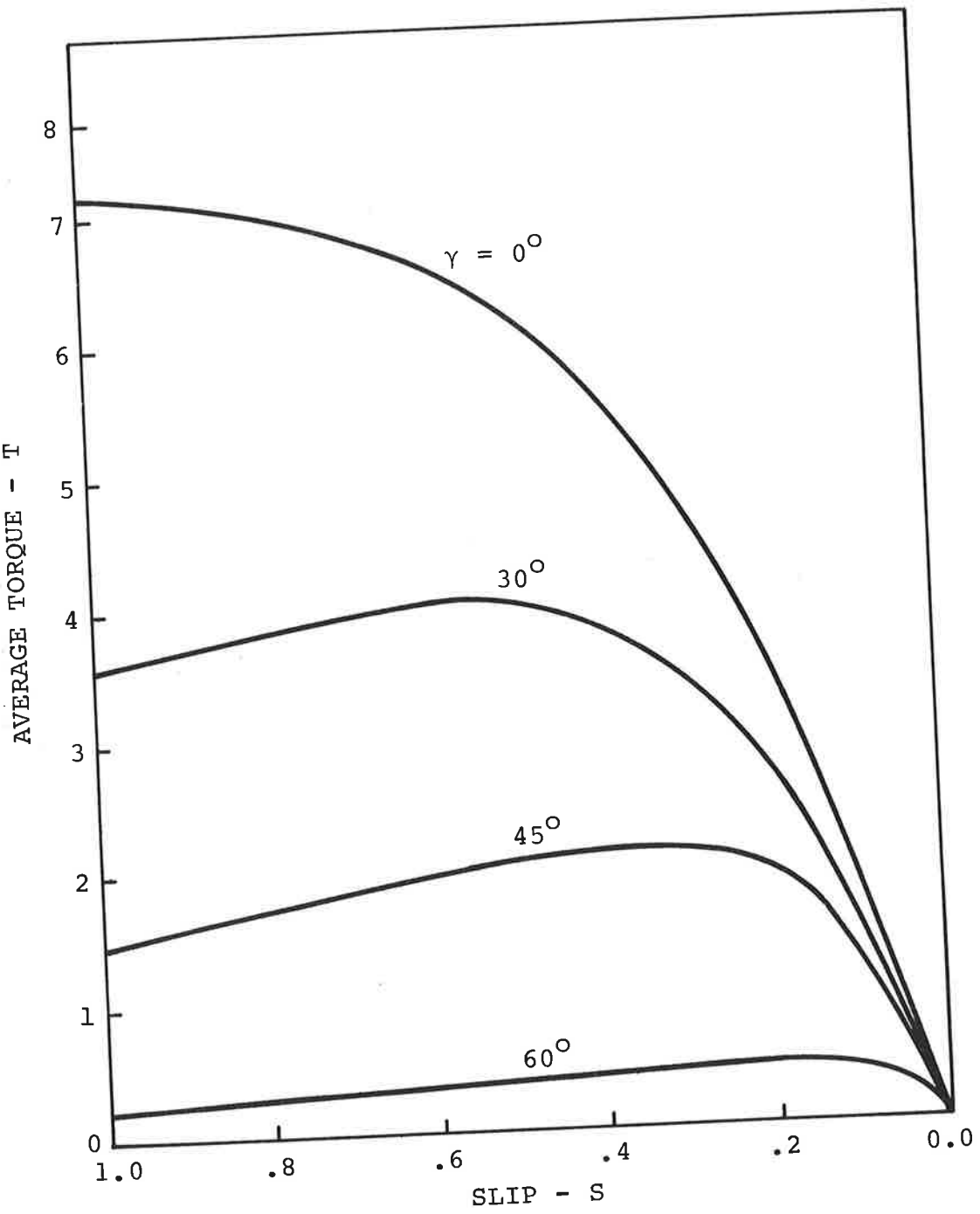

Figure 9. Torque-Slip Characteristic for Rotary Induction Motor #2

thyristor hold-off angles. As in the previous motor example, the peak average-torque shifts towards smaller values of slip with increasing hold-off angles. This is primarily attributable to the increase in the fundamental voltage harmonic with decreasing slip, which tends to make the fundamental current component and average torque independent of slip.

Current, Voltage, and Input Power Harmonics

The instantaneous phase current and phase voltage can be represented by Fourier series whose coefficients correspond to the amplitudes of the harmonic components. If spatial-harmonics are assumed absent, the current and voltage functions are given by

$$i(t) = \sum_n I(n)\cos\left[n\omega_s t+\phi_I(n)\right] \tag{13}$$

$$v(t) = \sum_n V(n)\cos\left[n\omega_s t+\phi_v(n)\right] \tag{14}$$

The coefficients in the above series are found by integrating the product of the respective time varying functions and the harmonic sinusoid function over a period. If advantage is taken of the rotational symmetry properties possessed by the 3-phase rotary induction motor, the Fourier coefficients, I(n), V(n), expressed in terms of d-q components are

$$C(n) = \frac{1}{N}\sqrt{\left[\sum_n c_q\cos\frac{n\pi}{3N} \mp c_d\sin\frac{n\pi}{3N}\right]^2 + \left[\sum_n c_q\sin\frac{n\pi}{3N} \mp c_d\cos\frac{n\pi}{3N}\right]^2} \tag{15}$$

where C(n) represents the generalized Fourier coefficient, c_p, c_q are the instantaneous d-q components, and N specifies the number of waveform samples taken in a $\pi/3$ phase interval. The upper and lower signs refer respectively to forward (3n+1) and backward (3n-1) propagating waves. The derivation of Equation 15 is given in Appendix B.

The primary current and phase voltage harmonics were computed according to Equation 15 for Motor #1 at 15 degree intervals of thyristor hold-off angle and slips of 0.1 and .03. Table 3 summarizes the harmonic amplitudes and phase displacement angles corresponding to the 1^{st}, 5^{th}, 7^{th}, 11^{th}, 13^{th}, and 17^{th} harmonics. The supply voltage was taken to be $\sqrt{2}\sin(\omega_s t+\phi_o)$, where ϕ_o is the phase angle defined in Figure 3. The phase angles $\phi_I(n)$, $\phi_v(n)$ measure the phase displacement of the current voltage harmonics given by Equations 13 and 14 with reference to the position of zero phase current. When normalized to the fundamental harmonic, the current harmonics are almost independent of slip in contrast to the voltage harmonics which depend markedly upon slip. A comparison of the 1^{st} harmonic amplitudes of the current and voltage for the thyristor hold-off angle of 60 degrees shows that while the current harmonic decreases by 22 percent in going from a slip of 1.0 to a slip of .03, the voltage harmonic increases 380 percent. This increase of the voltage fundamental with decreasing slip tends to make the current fundamental less dependent on slip.

The instantaneous input power can be expressed as

$$p(t) = \sum_v P(n)\cdot\cos\left(\phi_I(n)-\phi_v(n)\right)$$

$$+ \sum_n P(n)\cos\left(2n\omega_s t+\phi_I(n)+\phi_v(n)\right) \qquad (16)$$

$$P(n) = 0.5\ I(n)\cdot V(n)$$

Since the second term in the series is zero when averaged over a period, only the first term need by considered here. The last column in Table 4 labeled P_{real} gives the power harmonics associated with the time-independent term in Equation 16. The higher harmonics in general fall off rapidly with increasing harmonic order. However, at large hold-off angles, i.e., $\gamma = 60$ degrees, the 5^{th} harmonic component is not negligibly small compared with the fundamental. The power losses due to the

TABLE 3. HARMONIC AMPLITUDES AND PHASE DISPLACEMENT ANGLES COMPUTED FOR MOTOR #1

$$i(t) = \sum_{n=1}^{\infty} I(n)\cos\left(n\omega_s t + \phi_I(n)\right) \qquad v(t) = \sum_{n=1}^{\infty} V(n)\cos\left(n\omega_s t + \phi_v(n)\right)$$

$$P = \sum_{n=1}^{\infty} P_{real} \qquad v_{supply} = \sqrt{2}\sin(\omega_s t + \phi_o)$$

n	I(n)	$\phi_I(n)$	V(n)	$\phi_v(n)$	P(n)	$\phi_p(n)$	P_{real}
Hold-Off Angle (γ) = 15°		Slip (s) = 1.0		ϕ_o = 70.96°			
1	5.32	-97.3	1.07	-22.8	2.85	74.5	.765
5	.329	55.3	.322	142.0	.053	86.7	.003
7	.220	39.3	.301	127.0	.033	87.7	.0015
11	.113	8.1	.241	96.6	.014	88.5	.0003
13	.082	-7.4	.205	81.3	.008	88.7	.0002
17	.039	-38.4	.127	50.6	.003	89.0	-
Hold-Off Angle (γ) = 15°		Slip (s) = .03		ϕ_o = 48.47°			
1	1.360	-97.3	1.34	-13.0	.910	84.3	.091
5	.985	54.9	.082	141.6	.0035	86.7	.0002
7	.056	39.6	.077	127.5	.0022	87.9	.0001
11	.029	8.0	.062	96.5	.0009	88.5	-
13	.021	-7.2	.052	81.6	.0005	88.8	-
17	.010	-38.2	.032	50.9	.0002	89.1	-
Hold-Off Angle (γ) = 60°		Slip (s) = 1.0		ϕ_o = 58.53°			
1	.627	-119.7	.123	-45.2	.0386	74.5	.0105
5	.301	-58.3	.293	28.4	.044	86.7	.0026
7	.108	63.7	.147	151.4	.0080	87.7	.0003
11	.056	-60.1	.118	28.4	.0033	88.5	.0001
13	.034	62.7	.085	151.4	.0015	88.7	-
17	.023	-60.6	.075	28.4	.0008	89.0	-
Hold-Off Angle (γ) = 60°		Slip (s) = .03		ϕ_o = 48.8°			
1	.486	-114.8	.469	-30.5	.114	84.3	.0114
5	.233	-58.4	.227	28.3	.0265	86.7	.0015
7	.084	63.6	.114	151.5	.0048	87.9	.0002
11	.043	-60.1	.092	28.4	.0020	88.5	.0001
13	.026	62.5	.066	151.3	.0008	88.8	-
17	.018	-60.6	.058	28.5	.0005	89.1	-

TABLE 4. COMPARISON OF MEASURED AND COMPUTED CURRENT-VOLTAGE HARMONIC AMPLITUDES (FUNDAMENTAL HARMONIC AMPLITUDES NORMALIZED TO UNITY)

Hold-Off Angle = 60° Slip = 1.0

n	I_{theory}	$I_{meas.}$	V_{theory}	$V_{meas.}$
1	1.00	1.00	1.00	1.00
5	.480	.46	2.12	1.38
7	.173	.156	1.06	.71
11	.094	.083	.85	.55
13	.055	.029	.62	.23
17	.037	.017	.54	.05

Hold-Off Angle = 90° Slip = 1.0

n	I_{theory}	$I_{meas.}$	V_{theory}	$V_{meas.}$
1	1.00	1.00	1.00	1.00
5	.849	.81	3.99	2.86
7	.714	.56	4.68	2.62
11	.395	.24	4.04	1.67
13	.242	.144	2.91	.81
17	.013	.036	.119	.095

Hold-Off Angle = 60° Slip = .03

n	I_{theory}	$I_{meas.}$	V_{theory}	$V_{meas.}$
1	1.00	1.00	1.00	1.00
5	.480	.56	.194	.19
7	.173	.20	.098	.12
11	.089	.09	.078	.043
13	.055	.046	.056	.05
17	.037	.018	.049	.031

harmonics are greatest when the motor is operated at reduced input power levels by increasing the thyristor blocking angle.

An experimental study of harmonic phenomena occuring in a thyristor-controlled induction motor was next undertaken using the 15 hp rotary induction motor available in the Power and Propulsion Laboratory at TSC. The 1^{st}, 5^{th}, 7^{th}, 11^{th}, 13^{th}, and 17^{th} harmonic of line current and line-to-ground phase voltage were measured at the input terminals to the motor with the motor stopped and with the motor running at maximum speed. The latter measurement made under unloaded conditions corresponds to a slip of 0.03. The data of current harmonics were corrected for the low frequency dispersion of the current probe. In conjunction with the measurements, a computer analysis of the motor was undertaken based upon the impedance parameters given in the second section for Motor #3. While the computed voltage harmonics describe voltages developed across the phase windings and the measurements involve line-to-ground voltages, it can be shown that the neutral-to-ground voltage has no higher-harmonic which interacts with the primary current harmonics. Consequently, the amplitude to the neutral-to-ground voltage harmonics is zero for the harmonic orders with which we are concerned.

Table 4 summarizes the measured amplitudes of the current and voltage harmonics at unity slip for thyristor hold-off angles of 60 and 90 degrees and at a slip of 0.03 (unloaded motor) for the thyristor hold-off angle of 60 degrees. Also shown in the table are the computed harmonics for the same operating conditions. Good agreement exists between the computed and measured current harmonics, though the agreement between the corresponding voltage harmonics is only fair. A general correlation in the relative amplitude of the voltage harmonics with harmonic order is seen to exist, however. At unity slip, this correlation is improved considerably if the harmonic amplitudes are normalized to a larger fundamental harmonic. If allowance

is made for experimental errors and errors introduced by the choice of the particular impedance parameters used to describe the motor, the agreement between the computed and measured data is considered adequate.

The equivalent circuit of an induction motor at a harmonic frequency can be determined from measurements of amplitude of relative phase of the primary current and voltage harmonics. Since the impedance at a given harmonic is independent of the thyristor hold-off angle, the measurements can be made at reduced input power levels by increasing the thyristor hold-off angles. If the exciting current is neglected, then a measurement of amplitude and phase of the current and voltage at unity slip gives sufficient information to determine the total leakage reactances, $X_1 + X_2$, and the total input resistance, $R_1 + R_2$. The performance of the motor is affected relatively little by the way in which the total leakage reactance is distributed between primary and secondary.[4(p. 48)] By using available tables[11] giving an empirical distribution of the leakage reactance induction motors, the separate primary and secondary leakage reactance can be found. Since the primary resistance can be determined from a direct measurement of the stator resistance, subtracting this from the total input resistance yields the secondary resistance. The magnetizing reactance can be evaluated either by measuring the primary current under no-load conditions or by repeating the measurement of the current and voltage harmonic at no-load or at small motor slips. If separate tests are made at each harmonic frequency, the equivalent circuits of the induction motor can be found for each of the harmonic frequencies.

The amplitudes of the primary current harmonics, normalized to the fundamental harmonic at zero hold-off angle, are shown plotted in Figure 10 as a function of thyristor hold-off angle

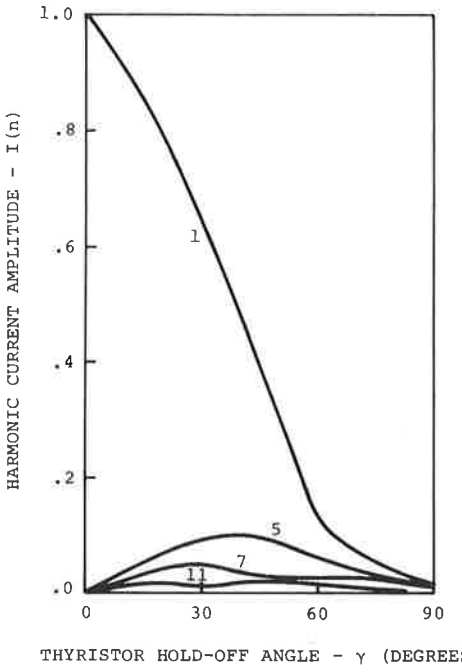

Figure 10. Amplitude of Primary Current Harmonics as a Function of Thyristor Hold-Off Angle Computed for Motor #1

for the case of Motor #1 with a slip of 0.2. The data is replotted in Figure 11 using the thyristor delay angle for the abscissa. Since the relative amplitudes of the harmonics are almost independent of slip for this example of a Class A motor, the data presented in the figures should be reasonably valid for all values of slip. At a hold-off angle of 45 degrees, the 5-th harmonic has a peak amplitude equal to 10 percent of the fundamental amplitude (at zero hold-off angle). Since torque is proportional to the square of the current, the contribution of the harmonic torques to the net average torque of the motor is expected to be very small.

The dependence of the fundamental primary current harmonic on the thyristor hold-off angle is presented in Figure 12 for Motor #1. At a slip, s = 1.0, the primary current harmonic decreases almost linearly with increasing hold-off angle, while at a slip, s = 0.0, the primary harmonic remains almost constant.

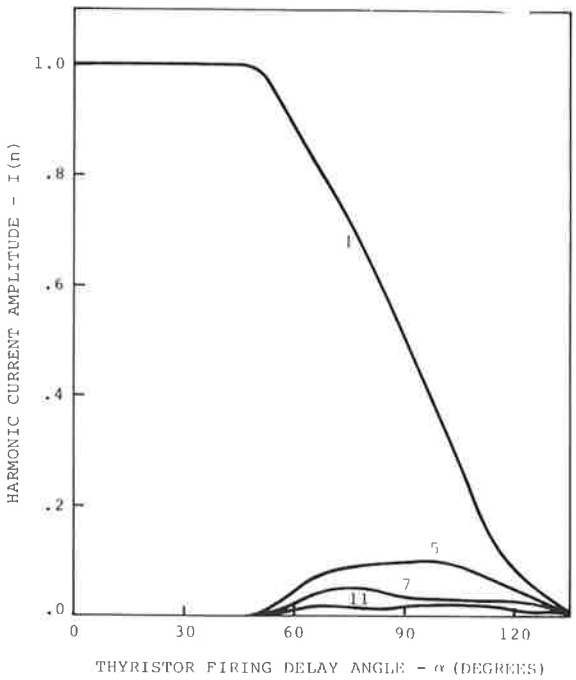

Figure 11. Amplitude of Primary Current Harmonics as a Function of Thyristor Firing-Delay Angle Computed for Motor #1

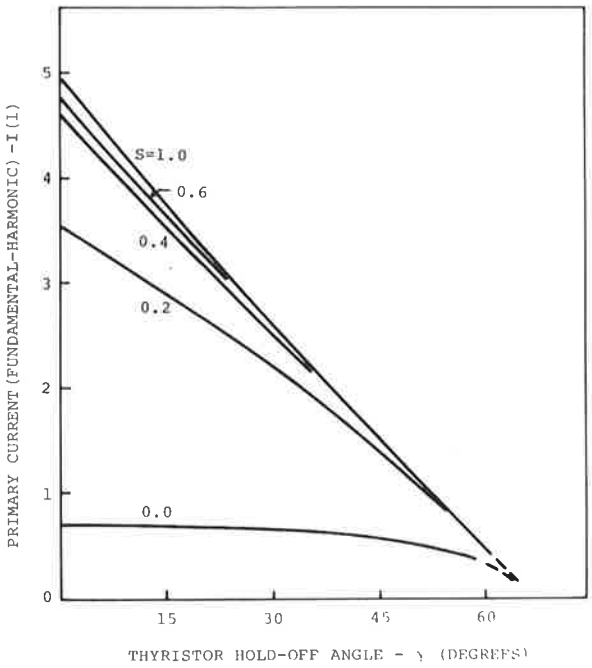

Figure 12. Amplitude of Primary Current Fundamental as a Function of Thyristor Hold-Off Angle Computed for Motor # 1

At hold-off angles approaching 60 degrees, the primary current is almost independent of slip. When the hold-off angle exceeds 60 degrees, or equivalently when the firing-delay angle is greater than 118 degrees, the primary current approaches zero.

Torque Harmonics

The torque harmonics can be found in the same manner used to determine the primary current harmonics, by resolving the instantaneous torque given by Equation 12 into its Fourier components using numerical integration. As an alternate method, the torque-harmonics, T(n), can be calculated from the known values of the primary current-harmonics, I(n), and the effective harmonic slip s* using,

$$T(n) = \frac{X_m^2 \left(R_2/_{S^*}\right) I_s^2(n)}{\left(\frac{R_2}{S^*}\right)^2 + \left(X_2+X_m\right)^2} \cdot \frac{3P}{\omega_s} \qquad (17)$$

The impedance parameters in the above equation are defined in Figure 1.

Table 5 lists the relative magnitudes of the torque harmonics (normalized to a fundamental amplitude of 100) computed for Motor #1 for thyristor hold-off angles of 15 and 60 degrees and slips equal to 0.1 and 0.9. As the table indicates, the higher-harmonic torques are extremely small compared with the fundamental, except at large hold-off angles and slips near unity. An induction motor operating at rated load and small slips would not be expected to be greatly affected by higher-harmonics. In such instances, an estimate of motor torque based on the fundamental harmonic should yield results which are reasonably accurate if the impedance parameters have been properly chosen for the induction motor.

TABLE 5. AMPLITUDE OF TORQUE HARMONICS COMPUTED FOR MOTOR #1 FOR THYRISTOR HOLD-OFF ANGLES OF 15 AND 60 DEGREES

n	Hold-Off Angle = 15°		Hold-Off Angle = 60°	
	Delay Angle = 85.1° s = 0.1	Delay Angle = 53.9° s = 0.9	Delay Angle = 111.6° s = 0.1	Delay Angle = 118.4° s = 0.9
1	100	100	100	100
5	.0073	.069	.44	4.19
7	.0032	.023	.057	.415
11	.00046	.0041	.0081	.072
13	.00024	.0019	.0032	.025
17	.00004	.0004	.0011	.0094

Rotary Induction Motor Output Characteristics

The computer program was written to provide data on the I^2R heating losses in the primary and secondary circuits, the mechanical output power of the motor, and motor efficiency for the different values of slip and thyristor hold-off and firing-delay angles. The computer results are summarized in Table 6 for the example of the Class A induction Motor #1. Only heating losses were included in the calculation of the motor efficiency. The motor efficiency is seen to decrease somewhat with the thyristor hold-off angle; this is due to the additional I^2R heating losses associated with the higher-harmonics.

SPATIAL HARMONICS IN ROTARY INDUCTION MOTOR

The subject of the harmonics in the airgap flux resulting from nonsinusoidal current distributions in 3-phase motor windings will now be considered. The primary current can be written quite generally in terms of a Fourier series whose coefficients are the Fourier components of the time- and space-harmonics

$$i_{as} = \sum_k \sum_n I_s(k,n) \cos\left(n\omega_s t - \frac{k\pi x}{\tau_p} + \delta(n,k)\right) \qquad (18)$$

TABLE 6. OUTPUT CHARACTERISTICS OF ROTARY INDUCTION MOTOR #1

Hold-Off Angle γ (degrees)	Delay Angle ϕ (degrees)	Slip	Stator Loss (p.u.)	Rotor Loss (p.u.)	Mech. Power (p.u.)	Average Torque (p.u.)	Efficiency (percent)
0	49.1	.2	.3239	.6064	2.4265	6.066	72.3
	62.1	.4	.5341	1.0172	1.5259	5.0864	49.6
	68.6	.4	.6152	1.1755	.7837	3.9184	30.4
	72.3	.8	.6524	1.2480	.3120	3.1200	14.1
	74.6	1.0	.6724	1.2870	.0000	2.5740	0.0
15	63.8	.2	.2357	.4413	1.7540	4.3850	72.1
	75.8	.4	.3397	.6471	.9643	3.2143	49.4
	81.2	.6	.3731	.7130	.4721	2.3606	30.3
	84.1	.8	.3873	.7410	.1840	1.8398	14.0
	86.0	1.0	.3947	.7555	.0000	1.5005	0.0
30	79.9	.2	.1400	.2623	1.0207	2.5519	71.7
	89.7	.4	.1757	.3346	.4882	1.6272	48.9
	93.7	.6	.1851	.3538	.2293	1.1463	29.8
	95.7	.8	.1889	.3614	.0878	.8777	13.8
	97.0	1.0	.1908	.3653	.0000	.7090	0.0
45	97.2	.2	.0554	.1039	.3875	.9688	70.9
	103.5	.4	.0615	.1172	.1638	.5461	47.8
	105.9	.6	.0629	.1202	.0745	.3726	28.9
	107.1	.8	.0634	.1213	.0281	.2814	13.2
	107.8	1.0	.0637	.1219	.0000	.2255	0.0
60	115.1	.2	.0067	.0127	.0391	.0978	66.9
	117.2	.4	.0069	.0131	.0151	.0505	43.1
	117.9	.6	.0069	.0132	.0067	.0336	25.0
	118.3	.8	.0069	.0132	.0025	.0250	11.0
	118.5	1.0	.0069	.0133	.0000	.0198	0.0

The amplitude of the torque harmonics for the case when higher spatial-harmonics are neglected was given by Equation 17. The corresponding expression[12] for the spatial-harmonic torque components when time-harmonics are assumed absent is

$$T(k) = 3P \frac{\left(X_m/k\right)^2 R_2 \left(\frac{\omega_s}{k} - \omega_m\right) \cdot I_s^2(k,s)}{R_2^2 + \left(\frac{X_2+X_m}{k}\right)^2 \left(\frac{\omega_s}{k} - \omega_m\right)^2} \qquad (19)$$

where ω_m is the angular velocity of the motor. The Fourier current harmonic, $I_s(k,s)$, of the primary current is a function of harmonic number k, and motor slip s. The sign of the harmonic torque is negative for flux waves propagating in the backward direction, i.e., k = 3n-1. The form of Equation 19 expresses the fact that both the speed of propagation and amplitude of the airgap flux wave vary inversely with harmonic number k.

The torque components associated with the phase-belt harmonics of a particular primary winding configuration will now be calculated. The primary winding is assumed to have a coil pitch of 2/3, and the number of poles equal to 5. The relative amplitude of the first eight winding current-harmonics in a 3-phase winding having zero current in one phase is[13]

I(1)=1.0 I(3)=0.0 I(5)=-.2 I(7)=-.14 I(9)=0.0

I(11)=-.09 I(13)=.078 (20)

The values of the harmonic amplitudes given above are based on a fundamental spatial wavelength equal to twice the pole pitch. A sketch of harmonic thrust T(k) versus slip computed for Motor #1 for the first several harmonics is shown in Figure 13. The largest contribution of the higher-harmonics to the average torque occurs near unity slip; for the Class A induction motor being considered, the reduction in torque at s = 1.0 amounts to almost 10 percent.

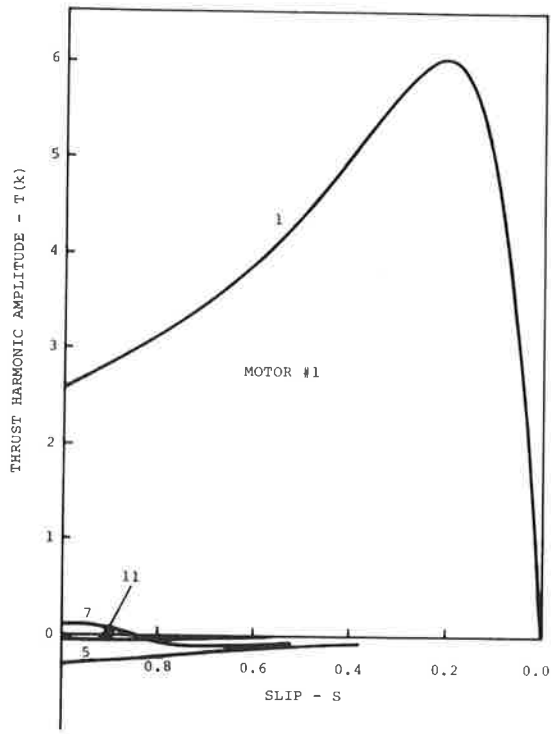

Figure 13. Amplitude of Thrust Harmonics as a Function of Slip

SPATIAL-HARMONICS IN LINEAR INDUCTION MOTORS

This section considers spatial harmonics in linear induction motors and their effect on the thrust developed by the motor. Spatial variations in the airgap flux density can result from nonsinusoidal winding current distributions (phase belt harmonics), perturbations in the magnetic permeance caused by changing airgap thickness (slot harmonics), and the decay of the airgap flux to zero in the region beyond the motor (end-effect). The latter factor will be the main concern of this section, since it represents one of the major effects contribution to nonuniform flux density in short primary type induction motors.

Figure 14 shows a sketch of the instantaneous flux in the airgap of a linear induction motor. The flux is assumed to consist of two waves, a normal wave of constant amplitude traveling at a speed U_1 with respect to the primary element, and an end-effect wave moving at motor speed with respect to the primary

element. The assumption of a constant speed U_2 for the end-effect wave is valid only in a high speed approximation.[2] (p.4) With respect to the secondary (reaction rail), the end-effect wave is stationary and typically described by a sinusoid function decaying exponentially with the distance from the motor end. The decay constant describing the propagation distance required for the end-effect wave to decay to 1/e of its initial amplitude will be taken to be

$$\alpha = T_2 U_2 = \frac{1}{\omega_s} \frac{(X_1+X_2)}{(R_1+R_2)} U_2 \qquad (21)$$

This expression for the damping constant was taken from the Garrett Report.[3] (p. 4-10)

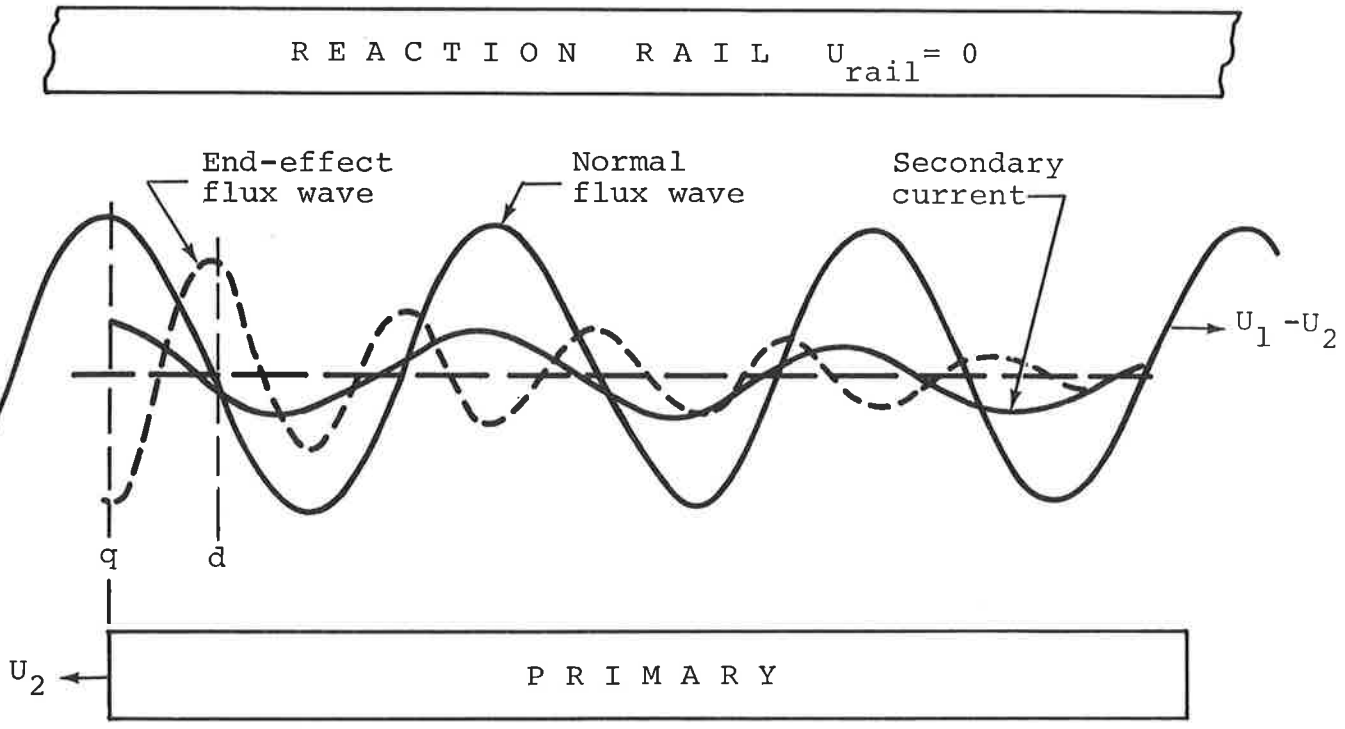

Figure 14. Schematic Showing Flux Distribution in Airgap of Linear Induction Motor.

Effective Secondary Resistance in the LIM

The instantaneous thrust developed by the linear induction motor is equal to the product of the instantaneous secondary current and airgap flux integrated over the length of the motor. The average thrust, found by integrating the instantaneous thrust over a period, can be equated to the ratio of power consumed in the effective secondary resistance $R_2'(1-s)/s$ to the velocity of the motor.

The effective secondary resistance associated with the motor thrust, assuming the absence of higher-harmonics (other than those comprised in the end-effect wave), is given by[3] (p. 4-15)

$$R_2' = R_2 \left[1 - \frac{1}{P\tau_p \cos\phi \, D} \left[e^{-P\tau_p / T_2 U_2} \sin\left(\frac{P\omega s}{1-s} - \theta_f \right) + \sin \theta_f \right] \right] \tag{22}$$

where P is the number of poles per side, τ_p is the pole pitch, R_2 is the static secondary resistance seen by the primary, and D is a quantity which depends on the motor slip. The term in the parentheses is primarily a function of the relative distance traveled by the end-effect wave, i.e., $T_2U_2/P\tau_p$, the slip, s, and the phase angle, θ_f given by

$$\theta_f = \tan^{-1} \frac{sX_2}{R_2} + \tan^{-1} \frac{1}{T_2 U_2} \tag{23}$$

The effective resistance associated with the heating losses in the secondary circuit is

$$R_2'' = R_2 \left[1 + 2\Delta \frac{Z_{2e}^2}{X_m^2} + \Delta \cdot \frac{Z_{2e}}{X_m} \frac{1}{1 - e^{-P\tau_p / T_2 U_2}} \right] \tag{24}$$

where the term in the parentheses is again primarily a function of the relative distance traveled by the end-effect wave.

Figure 15 gives R_2' and R_2'' as a function of motor slip for Motor #1 for different values of time constant T_2 as defined by Equation 21. At unity slip, the effective resistances R_2 and R_2 are equal and given by the static resistance R_2. As the slip decreases to zero, the effective resistance associated with the motor thrust R_2' decreases while the effective resistance associated with the heating losses in resistance characteristic representing Motor #1 corresponds to the curve with a time constant equal to .003.

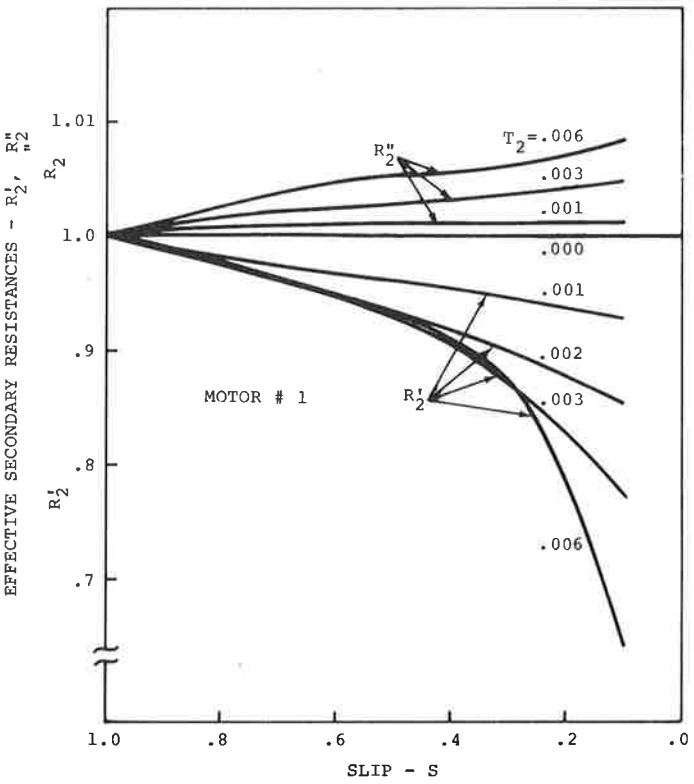

Figure 15. Effective Secondary Resistances, R_2' and R_2'', as a Function of Slip

An indication of the relative efficiency of a linear induction compared with a rotary induction motor can be obtained from Figure 15. If the approximation is made that the secondary current remains unchanged when the end-effect waves are included in the analysis, then the reduction in motor efficiency caused by the end-effect waves is directly proportional to the relative

decrease in the resistance R_2'. Referring to Figure 15, a substantial reduction in R_2' occurs at small motor slips with increasing time constant T_2. The lower motor efficiency when operated at rated load conditions suggests the advisability of using some form of compensating windings at the motor extremities to reduce the end-effect flux waves.

The dependence of motor thrust on T_2 is next explored. Figure 16 gives the thrust-slip characteristics of a LIM for different values of T_2 using the resistance functions presented in Figure 17 to describe the effective secondary resistance. The curve for $T_2 = 0.0$ corresponds to complete damping of the end-effect wave at the motor boundary. The decrease in motor thrust with increasing time-constant is largest at small slips. The shift in the position of peak thrust in the direction of larger slips is related to the greater effectiveness of the end-effect wave in reducing motor thrust at small slips.

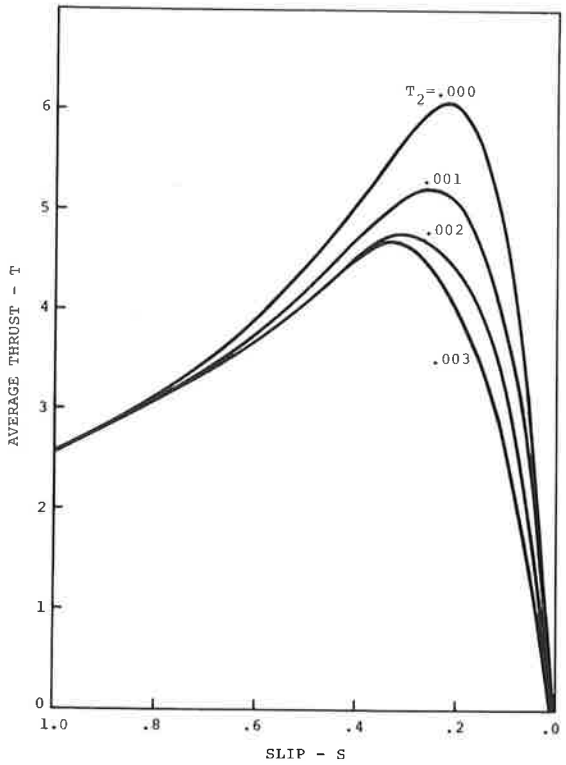

Figure 16. Thrust-Slip Characteristics of Motor #1 for Different Values of Time Constant T_2

TIME-HARMONICS IN THE LINEAR INDUCTION MOTOR

The output characteristics of a LIM controlled by symmetrically triggered thyristors will now be considered using the same mathematical approach adopted for the time-harmonic analysis of the rotary induction motor. The fixed impedance parameters which describe the secondary impedance of the rotary induction motor are replaced by their effective secondary impedance equivalents given by Equations 15 and 17. This greatly simplifies the calculations of the instantaneous motor currents but also introduces a slight error since the expressions for the effective resistances are exact only for the fundamental-harmonic. The magnitude of this error can be estimated from the data presented in Figure 8 together with the functional dependence of R_2' on motor slip as given by Equation 15. The maximum error in the value of the 5-th and 7-th resistance harmonics was estimated to be less than four percent; this is sufficiently small to be neglected in the calculation of average motor thrust.

The average thrust of the LIM was determined by first calculating the amplitude of the instantaneous secondary current using the secondary resistance given by $R_2'(1-s)/s+R_2''$ as shown in Figure 2. The instantaneous thrust was next computed based on the effective resistance (thrust) R_2' and the instantaneous values were then integrated over one period to give average thrust. Figure 17 shows the computed thrust-slip characteristics for the thyristor-controlled LIM based on the impedance parameters of Motor #1. The value of the time-constant, T_2, used in the calculations is 0.0033. A comparison of these thrust characteristics with the corresponding characteristics for the rotary induction motor (Figure 8) shows that the LIM has a lower thrust output in the region of small slips. The two motor characteristics approach the same limiting values at unity slip since the end-effect losses disappear in the thrust calculations for the LIM.

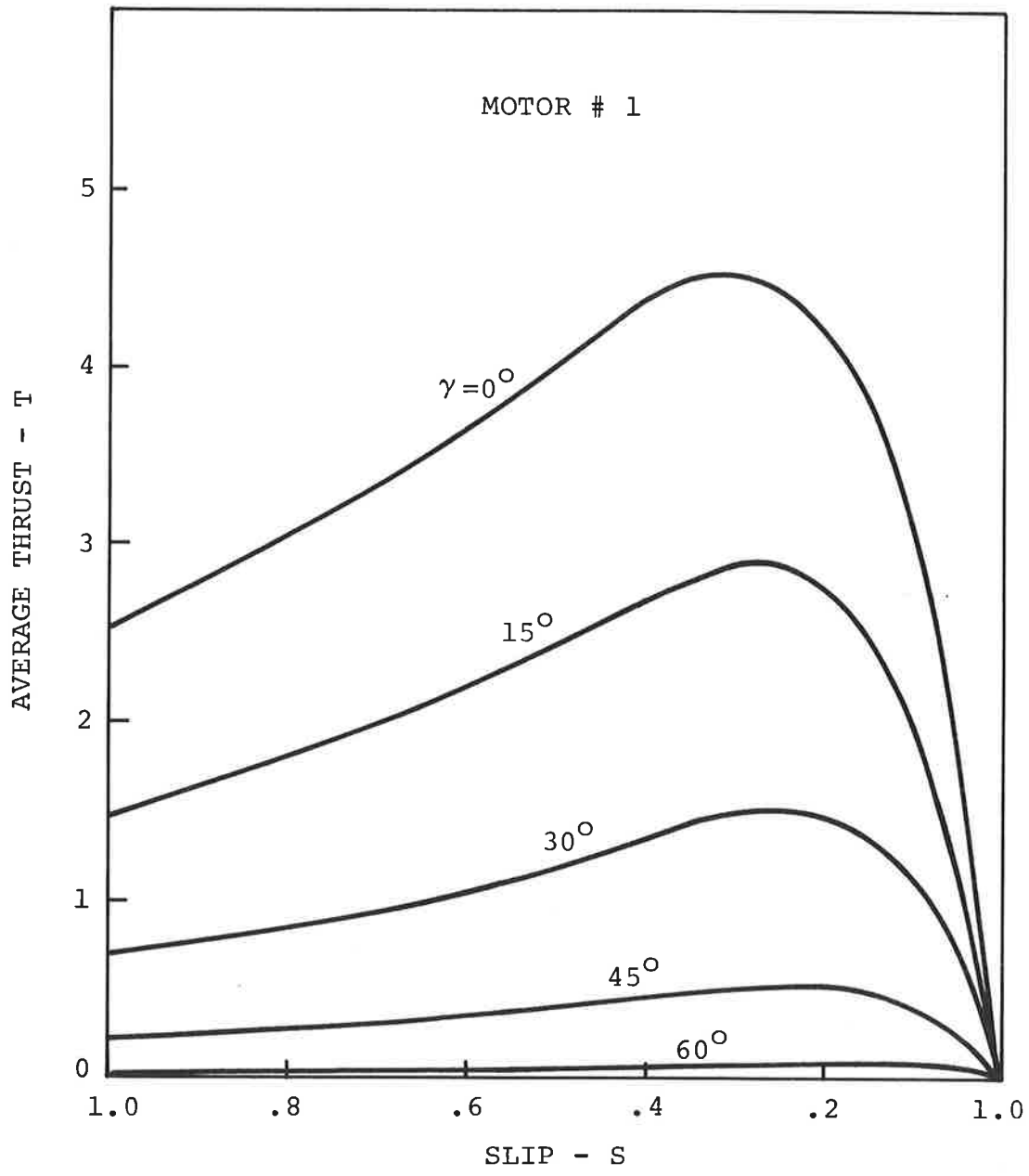

Figure 17. Thrust-Slip Characteristics of Linear Induction Motor with Thyristor-Control

CONCLUSIONS

The effect of time- and space-harmonics on the operating characteristics of rotary and linear induction motors has been considered in this report. The study has consisted of a theoretical analysis of the effect of harmonics on motor performance plus laboratory measurements of harmonics in a thyristor-controlled rotary induction motor. The results of the computer analysis and the results of the laboratory tests were found to be in reasonable agreement.

ROTARY INDUCTION MOTOR

A computer study was undertaken on a Wye-connected rotary induction motor to determine the dependence of motor torque on the harmonics present in the motor and to relate the motor output characteristics to changes in thyristor blocking angles (hold-off and firing-delay angles). The primary current and phase voltage waveforms were computed for different thyristor blocking angles and gave a visual indication of the amount of waveform distortion accompanying thyristor-control. A Fourier analysis of the current and voltage waveforms led to explicit values for the current and voltage harmonics. The current harmonics were found to be almost independent of motor slip, while the corresponding voltage harmonics were found to vary considerably with motor slip. The decrease in the current fundamental was seen to be approximately proportional to an increase in the thyristor firing-delay angle.

The average torque becomes relatively small for thyristor hold-off angles exceeding 60 degrees. In general, the amplitude of the harmonic torques are much less than the amplitude of the fundamental torque and cause only a slight reduction in the net average motor torque. Under most adverse conditions, namely small motor speeds and large thyristor hold-off angles, the higher torque harmonics cause a reduction of 3 to 5 percent in

motor efficiency for the machine examples considered in this report. The motor losses were mainly attributable to increases in heating losses in the primary and secondary circuits caused by the harmonic currents.

The torque-slip characteristics of an induction motor with thyristor-control are different in form from those with line voltage-control. In the latter case, the position of peak average-torque remains fixed when the line voltage is varied, while in the former case the position of peak average-torque shifts toward smaller slips with increasing thyristor hold-off angles. In addition, at large hold-off angles approaching 60 degrees, the average torque tends to remain constant and independent of slip. This behavior is attributable to the increase in voltage fundamental with increasing motor speed which causes the primary current fundamental to remain almost constant with slip.

The measurement of current and voltage harmonics at reduced power levels offers a convenient means for determining the impedance parameters in the equivalent circuit of the motor. Since the motor parameters are independent of the means used to control the motor, thyristors can be used to reduce the input power to the motor. By making two separate measurements of the primary current and voltage harmonics, one at unity slip and the other under no-load conditions, sufficient data is available to evaluate the impedance parameters of the motor. Measurements made at each harmonic frequency permit the motor characteristics to be defined by equivalent circuits valid at each frequency.

LINEAR INDUCTION MOTOR

The subject of the end-effect flux waves and their effect on the thrust-slip characteristics of a linear induction motor has been considered. It is shown that the end-effect wave can be described in terms of an effective secondary resistance which

is both slip and frequency dependent. This effective secondary resistance is equal to the static secondary resistance at a slip of unity, but becomes smaller in value as the motor slip is reduced. The two factors governing the propagation of the end-effect wave are the damping constant, which defines the extent of wave propagation along the airgap region of the motor, and the propagation wavelength, which determines the speed of the end-effect wave. The effective secondary resistance was computed for different values of damping constant and a family of resistance characteristics was presented to illustrate the dependence of this resistance on damping constant.

The thrust-slip characteristics of a Class A linear induction motor were computed for different damping constants (time constants) and showed the large decrease in motor thrust caused by the end-effect waves. The largest reduction in motor thrust occurs at small slips. As a result, motors operating at full speed or at rate load will be most adversely affected by the end-effect waves.

A family of thrust-slip curves were computed for a thyristor-controlled Class A linear induction motor using the same mathematical approach previously applied to analyze the rotary induction motor. The end-effect contribution was included in the analysis by substituting for the static secondary resistance term, the effective secondary resistance described above. This procedure offers one means for including both space- and time-harmonics in the mathematical treatment of the linear induction motor. It is hoped that the results can be used as a guide in estimating the thrust developed by a thyristor-controlled linear induction motor.

GLOSSARY OF SYMBOLS

C	Number of series conductors per phase per side
C(n)	Generalized Fourier coefficient in Fourier expansion of instantaneous current, voltage, and power, defined by Equation 16
I	Current vector (4-dimensional) formed from primary current i_1 and secondary current i_2 (referred to primary) given by $I = \left[i_1 \; i_2\right]^T = \left[i_{qs} \; i_{ds} \; i_{qr} \; i_{dr}\right]^T$
I_1	Amplitude of primary phase current, amperes
I_2	Amplitude of secondary phase current, referred to primary, amperes
k	Order of spatial-harmonic
$K_w(n)$	Primary winding factor associated with n-th harmonic
l_1	Primary stack length, meters
L_{22}	Secondary leakage inductance per phase in terms of the secondary in henries per meter of motor length per meter of stack
n	Order of frequency-harmonic
p	Instantaneous power, defined by Equation 15, watts
P	Number of poles
R	Resistance matrix (4x4 dimensional) defined by Equation A-5 in Appendix A
R_1	Primary resistance per phase, ohms
R_2	Secondary resistance per phase, referred to primary ohms
R_2'	Effective secondary resistance component associated with motor thrust, referred to primary, ohms

R''_2	Effective secondary resistance component associated with secondary heating losses, referred to primary, ohms
s	Motor slip
s*	Effective motor slip at harmonic frequency
t	Time, seconds
T	Torque, newton meters
T_2	Secondary time constant, seconds
U_1	Synchronous motor speed, meters per second
U_2	Motor speed, meters per second
v_{as}, v_{bs}, v_{cs}	Primary phase voltage across windings a, b, and volts
v_{ar}, v_{br}, v_{cr}	Secondary phase voltage across windings a, b, and c, volts
V	Voltage vector (2 dimensional) having components v_q and v_d along q and d coordinate axes
X	Reactance matrix (4x4 dimensional) defined by Equation A-4 in Appendix A
X_1	Primary leakage reactance per phase, ohms
X_2	Secondary leakage reactance per phase referred to primary, ohms
X_m	Magnetizing reactance per phase, ohms

α	Thyristor delay angle, defined in Figure 3, radians per second
γ	Thyristor hold-off angle, defined in Figure 3
δ	Phase displacement angle, defined by Equation 18, radians
β	Thyristor half-conduction angle, defined in Figure 3, radians per second
θ_f	Phase displacement angle, defined by Equation 23, radians
λ	Eigenroots of characteristic matrix A
λ_r	Real part of complex eigenroot λ
λ_i	Imaginary part of complex eigenroot λ
ρ_2	Secondary surface resistivity or resistance of a secondary element 1 meter wide in the x-direction one-half the secondary thickness in the y-direction and one inch long in the z-direction
τ_p	Pole pitch of motor, meters
ϕ	Phase angle, defined in Figure 3, radians per second
$\phi_i(n)$, $\phi_v(n)$, $\phi_p(n)$	Phase displacement angles, defined by Equations 13, 14, and 16
ω_m	Motor angular frequency, radians per second
ω_s	Synchronous angular frequency, radians per second

APPENDIX A
MATRIX EQUATIONS DESCRIBING THYRISTOR-CONTROLLER INDUCTION MOTOR

The determination of the instantaneous phase current over a time interval of one period requires separate solutions of Equation 4 for each System State. If the current and phase voltage are written as vector

$$x = \begin{bmatrix} i_{qs} \\ i_{ds} \\ i_{qr} \\ i_{dr} \end{bmatrix} \tag{A-1}$$

$$v = \begin{bmatrix} v_{qs} \\ v_{ds} \\ v_{qr} \\ v_{dr} \end{bmatrix} = \begin{bmatrix} v_{qs} \\ v_{ds} \\ 0 \\ 0 \end{bmatrix} \tag{A-2}$$

Equation 4 takes the following form in System States 1, 2, and 3.

System State 1

$$\frac{dx}{dt} = - X_1 \cdot R \cdot x + X^{-1} \cdot v \tag{A-3}$$

$$X_1 = \begin{bmatrix} x_s & 0 & x_m & 0 \\ 0 & x_s & 0 & x_m \\ x_m & 0 & x_r & 0 \\ 0 & x_m & 0 & x_r \end{bmatrix} \tag{A-4}$$

$$R = \begin{bmatrix} R_1 & 0 & 0 & 0 \\ 0 & R_1 & 0 & 0 \\ 0 & -(1-s)x_m & R_2 & -(1-s)x_r \\ (1-s)x_m & 0 & (1-s)x_r & R_2 \end{bmatrix} \qquad \text{(A-5)}$$

System State 2

$$\frac{dx}{dt} = - X_2 \cdot R \cdot x + X_2^{-1} \cdot v$$

$$X_2 = \begin{bmatrix} x_s & 0 & 0 & 0 \\ 0 & x_s & 0 & x_m \\ x_m & 0 & x_r & 0 \\ 0 & x_m & 0 & x_r \end{bmatrix} \qquad \text{(A-6)}$$

System State 3

$$\frac{dx}{dt} = - X_3^{-1} \cdot R \cdot x + X_3^{-1} \cdot v$$

$$X_3 = \begin{bmatrix} x_s & 0 & 0 & 0 \\ 0 & x_s & 0 & 0 \\ x_m & 0 & x_r & 0 \\ 0 & x_m & 0 & x_r \end{bmatrix} \qquad \text{(A-7)}$$

APPENDIX B
DERIVATION OF EQUATIONS FOR CURRENT AND VOLTAGE HARMONIC AMPLITUDES

The instantaneous current and phase voltage can be expressed by the Fourier series

$$i = \sum_{n=0}^{\infty} \left(A_i(n) \cos \frac{2\pi nm}{M} + B_i(n) \sin \frac{2\pi nm}{M} \right) \qquad \text{(B-1)}$$

$$v = \sum_{n=0}^{\infty} \left(A_v(n) \cos \frac{2\pi nm}{M} + B_v(n) \sin \frac{2\pi nm}{M} \right) \qquad \text{(B-2)}$$

where M is the number of equally spaced time intervals in one period, m is an integer which varies from 1 to M and specifies the waveform sampler number, n is the harmonic number, and A(n), B(n) are the amplitude coefficient of the Fourier series. For a 3-phase Wye connected motor the current in a given phase winding over a 2π phase interval can be written in terms of the d-q current components valid in a $\pi/3$ phase interval according to

$$i(\omega t) = i_q \qquad 0 \leq \omega t \leq \pi/3 \qquad \text{(B-3)}$$

$$i(\omega t) = \frac{i_q}{2} + \frac{\sqrt{3}}{2} i_d \qquad \frac{\pi}{3} \leq \omega t \leq \frac{2\pi}{3} \qquad \text{(B-4)}$$

$$i(\omega t) = -\frac{i_q}{2} + \frac{\sqrt{3}}{2} i_d \qquad \frac{2\pi}{3} \leq \omega t \leq \pi \qquad \text{(B-5)}$$

$$i(\omega t) = - i_q \qquad \pi \leq \omega t \leq \frac{4}{3}\pi \qquad \text{(B-6)}$$

$$i(\omega t) = -\frac{i_q}{2} - \frac{\sqrt{3}}{2} i_d \qquad \frac{4\pi}{3} \leq \omega t \leq \frac{5}{3}\pi \qquad \text{(B-7)}$$

$$i(\omega t) = \frac{i_q}{2} - \frac{\sqrt{3}}{2} i_d \qquad \frac{5\pi}{3} \leq \omega t \leq 2\pi \qquad \text{(B-8)}$$

The Fourier coefficients in Equation B-1 are given by

$$A_i(n) = \frac{\sum_{m=1}^{M} i \cdot \cos \frac{2\pi nm}{M}}{\sum_{m=1}^{M} \cos^2 \frac{2\pi nm}{M}} \qquad \text{(B-9)}$$

$$B_i(n) = \frac{\sum_{m=1}^{M} i \cdot \sin \frac{2\pi nm}{M}}{\sum_{m=1}^{M} \sin^2 \frac{2\pi nm}{M}} \qquad \text{(B-10)}$$

Now

$$\sum_{m=1}^{M} \cos^2 \frac{2\pi nm}{M} = \sum_{m=1}^{M} \sin^2 \frac{2\pi nm}{M} = \frac{M}{2} \qquad \text{(B-11)}$$

Substituting (B-3) through (B-8) in (B-9) and (B-10) and making use of the fact that $i(\omega t+\pi) = - i(\omega t)$

$$\begin{aligned} A_i(n) = \frac{4}{M} \sum_{m=1}^{M/6} \Bigg\{ \cos \frac{2\pi nm}{M} \Bigg[i_q + \left(\frac{i_q}{2} + i_d \frac{\sqrt{3}}{2} \right) \cos \frac{n\pi}{3} \\ + \left(- \frac{i_q}{2} - \frac{\sqrt{3}}{2} i_d \right) \cos \frac{n2\pi}{3} \Bigg] \\ + \sin \frac{2\pi nm}{M} \Bigg[\left(- \frac{i_q}{2} - \frac{\sqrt{3}}{2} i_d \right) \sin \frac{n\pi}{3} \\ + \left(\frac{i_q}{2} - \frac{\sqrt{3}}{2} i_d \right) \sin \frac{n2\pi}{3} \Bigg] \Bigg\} \end{aligned} \qquad \text{(B-12)}$$

$$B_i(n) = \frac{4}{M} \sum_{m=1}^{M/6} \left\{ \sin \frac{2\pi nm}{M} \left[i_q + \left(\frac{i_q}{2} + \frac{\sqrt{3}}{2} i_d \right) \cos \frac{n\pi}{3} \right. \right. \quad \text{(B-13)}$$

$$\left. + \left(-\frac{i_q}{2} + \frac{\sqrt{3}}{2} i_d \right) \cos \frac{n2\pi}{3} \right]$$

$$+ \cos \frac{2\pi nm}{M} \left[\left(\frac{i_q}{2} + \frac{\sqrt{3}}{2} i_d \right) \sin \frac{n\pi}{3} \right.$$

$$\left. \left. + \left(-\frac{i_q}{2} + \frac{\sqrt{3}}{2} i_d \right) \sin \frac{n2\pi}{3} \right] \right\}$$

Equations B-12 and B-13 reduce to

$$A_i(n) = \frac{1}{N} \sum_{m=1}^{N} \left[i_q \cos \frac{m\pi}{3N} \pm i_d \sin \frac{m\pi}{3N} \right] \text{ when } n = 1,7,13,\cdots \quad \text{(B-14)}$$

$$A_i(n) = \frac{1}{N} \sum_{m=1}^{N} \left[i_q \cos \frac{m\pi}{3N} \mp i_d \sin \frac{m\pi}{3N} \right] \text{ when } n = 5,11,17,\cdots$$

$$B_i(n) = \frac{1}{N} \sum_{m=1}^{N} \left[i_q \sin \frac{m\pi}{3N} \mp i_d \cos \frac{\pi m}{3N} \right] \text{ when } n = 1,7,13,\cdots \quad \text{(B-15)}$$

$$B_i(n) = \frac{1}{N} \sum_{m=1}^{N} \left[i_q \sin \frac{m\pi}{3N} \pm i_d \cos \frac{\pi m}{3N} \right] \text{ when } n = 5,11,17,\cdots$$

where $N = \frac{M}{6}$ is the number of samples (taken at equal intervals) of current i taken in a $\pi/3$ phase interval.

The amplitude of the n-th harmonic current is

$$I(n) = \sqrt{A_i^2(n) + B_i^2(n)} \quad \text{(B-16)}$$

$$= \frac{1}{N} \sqrt{\left[\sum_{m=1}^{N} \left(i_q \cos \frac{m\pi}{3N} \mp i_d \sin \frac{m\pi}{3N} \right) \right]^2 + \left[\sum_{m=1}^{N} \left(i_q \sin \frac{m\pi}{3N} \pm i_d \cos \frac{m\pi}{3N} \right) \right]^2}$$

A corresponding expression in terms of the d-q phase voltage components gives the amplitude of the n-th harmonic of phase voltage.

REFERENCES

1. Largiader, H., "Design Aspects of Induction Motors for Traction Applications with Supply through Static Frequency Changer," Brown Boveri Rev., Vol. 70, pp. 152-167, April, 1970.

2. Yamamura, S., Ito, H., and Ishikawa, Y., "Theories of the Linear Induction Motor and Compensated Linear Induction Motor," IEEE Winter Conference on Rotating Machinery, Jan. 30, 1972, New York, N. Y.

3. "Study of Linear Induction Motor and its Feasibility for High-Speed Ground Transportation," Final Report by Garrett Corporation, 67-1948, June 1967. PB-174866 (pp.3-3).

4. Fitzgerald, A. E., and Kingsley, Jr., C., Electric Machinery, McGraw Hill, New York, 1961, pp. 291.

5. Alger, P. L., The Nature of Induction Machines, Gordon and Breach, New York, 1965. pp. 82.

6. "Dynamic Braking of the Urban Tracked Air Cushion Vehicle Alexander Kusko, Inc., Sept. 15, 1971, DOT Contract No. DOT-TSC-203.

7. Lipo, T. A., "The Analysis of Induction Motors with Voltage Control by Symmetrically Triggered Thyristors," IEEE Trans. Power Apparatus and Systems, Vol. PAS-90, No. 2, pp. 515-523, March/April 1971, pp. 521.

8. Private communication, Howell Electric Co.

9. Krause, P. C., and Thomas, C. H., "Simulation of Symmetrical Induction Machinery," IEEE Trans. Power Apparatus and Systems, Vol. PAS-84, No. 11, pp. 1038-1053, November 1965, pp. 1041.

10. Franklin, J. N., Matrix Theory, Prentice-Hall, Inc., Englewood Cliffs, N. J., 1968.

11. AIEE Test Code of Empirical Distribution of Leakage Reactances in Induction Motors.

12. Boon-Teck OOI, "Fringe-End-Effects of Short Stator," MIT Thesis, Dept of Electrical Eng., 1966, pp. 26.

13. Jayawant, B. V., Induction Machines, McGraw Hill, London, 1968, pp. 57.